

Argonne National Laboratory

**LOCAL PARAMETERS IN
COCURRENT MERCURY-NITROGEN FLOW**

by

L. G. Neal

LEGAL NOTICE

This report was prepared as an account of Government sponsored work. Neither the United States, nor the Commission, nor any person acting on behalf of the Commission:

- A. Makes any warranty or representation, expressed or implied, with respect to the accuracy, completeness, or usefulness of the information contained in this report, or that the use of any information, apparatus, method, or process disclosed in this report may not infringe privately owned rights; or*
- B. Assumes any liabilities with respect to the use of, or for damages resulting from the use of any information, apparatus, method, or process disclosed in this report.*

As used in the above, "person acting on behalf of the Commission" includes any employee or contractor of the Commission, or employee of such contractor, to the extent that such employee or contractor of the Commission, or employee of such contractor prepares, disseminates, or provides access to, any information pursuant to his employment or contract with the Commission, or his employment with such contractor.

ANL-6625
Engineering and Equipment
(TID-4500, 19th Ed.)
AEC Research and
Development Report

ARGONNE NATIONAL LABORATORY
9700 South Cass Avenue
Argonne, Illinois

LOCAL PARAMETERS IN COCURRENT MERCURY-NITROGEN FLOW

by

L. G. Neal
Northwestern University

Reactor Engineering Division, ANL,
and
Associated Midwest Universities

January 1963

This report is the first of a series that describes heat-transfer and fluid-flow studies performed at Argonne under a program sponsored jointly by the Associated Midwest Universities and the Argonne National Laboratory.

Operated by The University of Chicago
under
Contract W-31-109-eng-38
with the
U. S. Atomic Energy Commission

TABLE OF CONTENTS

| | <u>Page</u> |
|--|-------------|
| ABSTRACT | 7 |
| I. INTRODUCTION | 7 |
| II. REVIEW OF THE LITERATURE | 9 |
| III. A MODIFICATION OF THE VARIABLE-DENSITY MODEL TO INCLUDE LOCAL SLIP | 23 |
| IV. EXPERIMENTAL APPARATUS | 26 |
| A. Flow System | 26 |
| 1. Components | 26 |
| a. Mercury-Nitrogen Mixer | 26 |
| b. Test Section | 26 |
| c. Separator | 27 |
| d. Mercury Storage Tank | 27 |
| 2. Instrumentation and Control | 28 |
| a. Orifice Meters | 28 |
| b. Pressure Measurements | 28 |
| c. Temperature Measurements | 28 |
| d. Flow Control | 28 |
| 3. Procedure | 28 |
| B. Electric Probe | 29 |
| 1. Definition of Variables | 31 |
| 2. Method | 33 |
| 3. Signal Analysis | 35 |
| 4. Procedure | 36 |
| 5. Discussion | 36 |
| C. Impact Probe | 38 |
| 1. Method | 39 |
| 2. Calibration | 41 |
| 3. Procedure | 41 |
| 4. Discussion | 42 |

TABLE OF CONTENTS

| | <u>Page</u> |
|--|-------------|
| V. RESULTS AND DISCUSSIONS | 43 |
| A. Gas Fraction and Liquid Velocity Profiles | 44 |
| B. Average Velocities | 48 |
| C. Bubble Diameter and Slug Length Spectra | 49 |
| D. Slug Velocities | 58 |
| VI. CONCLUSIONS. | 60 |
| APPENDIX A: TABULATED DATA. | 61 |
| BIBLIOGRAPHY. | 69 |
| ACKNOWLEDGEMENTS | 73 |

LIST OF FIGURES

| No. | Title | Page |
|-----|---|------|
| 1. | Mercury-Nitrogen Flow System | 26 |
| 2. | Mercury-Nitrogen Mixer | 27 |
| 3. | Test Section | 27 |
| 4. | Mercury Storage Tank. | 27 |
| 5. | Electric Probe. | 33 |
| 6. | Photographic Record of Electric Probe Signal. | 33 |
| 7. | Integrating Circuit | 35 |
| 8. | Average Gas Fraction from Integration of Profile and from Measured Pressure Gradient | 37 |
| 9. | Impact Probe. | 39 |
| 10. | Schematic of Differential Pressure-Measuring System | 40 |
| 11. | Typical Gas Fraction Profiles at $\xi = 5.7$ | 44 |
| 12. | Developing Gas Fraction Profiles for Increasing Values of β | 44 |
| 13. | Gas Fraction Profiles at $\xi = 28.5$ and $\xi = 51.5$ for Varying β and Constant $Re^* = 2.6$ | 45 |
| 14. | Gas Fraction Profiles at $\xi = 28.5$ and $\xi = 51.5$ for Varying Re^* and Constant $\beta = 0.3$ | 45 |
| 15. | Liquid Velocity Profiles at $\xi = 5.7$ for Large Re^* and Increasing β | 46 |
| 16. | Liquid Velocity Profiles at $\xi = 28.5$ and $\xi = 51.5$ for Varying β and Constants $Re^* = 13.6$ | 46 |
| 17. | Liquid Velocity Profiles for $\beta = 0.3$ and Varying Re^* | 46 |
| 18. | Bubble Size Distribution at $\xi = 5.7$ | 50 |
| 19. | Bubble Size Distribution at $\xi = 28.5$ | 51 |
| 20. | Bubble Size Distribution at $\xi = 51.5$ | 52 |
| 21. | Gas Slug Length Distribution at $\xi = 28.5$ | 53 |
| 22. | Gas Slug Length Distribution at $\xi = 51.5$ | 54 |
| 23. | Liquid Slug Length Distribution at $\xi = 51.5$ | 55 |
| 24. | Comparison of Liquid Slug Length Distributions at $\xi = 28.5$ and $\xi = 51.5$ | 56 |
| 25. | Time Average Slug Shapes | 57 |
| 26. | Nitrogen Slugs in Stagnant Mercury | 59 |

LIST OF TABLES

| No. | Title | Page |
|------|--|-------|
| I. | Calibration of Impact Probe | 41 |
| A-1. | Gas Fraction | 62-65 |
| A-2. | Liquid Velocity | 66 |
| A-3. | Calculated Profile Data | 66 |
| A-4. | Armand's Parameter | 67 |
| A-5. | Average and Slip Velocity Data | 68 |

NOMENCLATURE

| | |
|-------------|--|
| A_p | pipe cross-sectional area, ft^2 |
| $B(\xi)$ | cumulative bubble size distribution function |
| $b(\xi)$ | density function for bubbles of diameter ξ |
| C | electrical capacitance, farads; Armand's parameter, α/β |
| D_p | pipe diameter, ft |
| D_B | bubble diameter, ft |
| E | electrical voltage, v |
| $e(t)$ | voltage signal from electrical probe, v |
| Fr | Froude number |
| $G(\xi)$ | cumulative gas slug length distribution function |
| $g(\xi)$ | density function for gas slugs of length ξ |
| K | Constant, $\Omega_n \Omega_p / \Omega_{np}$ |
| $L(\xi)$ | cumulative liquid slug length distribution function |
| $l(\xi)$ | density function for liquid slugs of length ξ |
| n | positive constant |
| P | Pressure, lb/ft^2 or kg/cm^2 |
| p | positive constant |
| Q_G | gas volumetric flow rate, ft^3/sec |
| Q_L | liquid volumetric flow rate, ft^3/sec |
| R | pipe radius, ft; electrical resistance, ohms |
| Re | Reynolds number |
| r | pipe radius variable, ft |
| S | dimensionless variable distance from the pipe wall, y/R |
| T | Temperature, $^{\circ}C$; integration time, sec |
| t | variable time, sec |
| U_L | local liquid velocity, ft/sec |
| \bar{U}_L | cross-sectional average liquid velocity, ft/sec |
| U_G | local gas velocity, ft/sec |
| \bar{U}_G | cross-sectional average gas velocity, ft/sec |

| | |
|-----------|--|
| U_B | bubble velocity, ft/sec |
| U_s | slug velocity, ft/sec |
| u_L | liquid slip velocity, ft/sec |
| u_G | gas slip velocity, ft/sec |
| u_R | relative slip velocity, ft/sec |
| V_{Mix} | mixture velocity, ft/sec |
| W_G | gas mass flow rate, lb/sec |
| W_L | liquid mass flow rate, lb/sec |
| W_T | total mass flow rate, lb/sec |
| We | Weber number |
| x | steam quality |
| y | variable distance from tube wall, $(r - r)$, ft |
| z | variable distance along channel length, ft |

Greek

| | |
|----------------|--|
| α | local gas fraction |
| $\bar{\alpha}$ | cross-sectional average gas fraction |
| α_m | maximum gas fraction |
| β | gas volumetric flow fraction |
| δ | liquid film thickness, ft |
| ξ | dimensionless bubble diameter, D_B/D_P , or slug length |
| η | average phase velocity ratio |
| θ_B | dwelt time of a bubble, sec |
| λ | contribution to the average phase velocity ratio resulting from non-uniform phase distribution |
| μ | viscosity, lb/(ft)(sec) |
| ξ | dimensionless distance from test section inlet, z/D_P |
| ρ_G | gas density, lb/ft ³ |
| ρ_L | liquid density, lb/ft ³ |
| ρ | mixture density, lb/ft ³ |
| Φ | local phase velocity ratio |

LOCAL PARAMETERS IN COCURRENT MERCURY-NITROGEN FLOW

by

L. G. Neal

ABSTRACT

Two instruments were developed which can be used to study the structure of two-phase flow: first, an electrical probe capable of measuring local values of the gas fraction, bubble frequency, and bubble-size spectra; second, an impact probe that can be used to measure the local liquid velocity.

These instruments were used to measure local flow parameters in cocurrent mercury-nitrogen slug flow. These results are presented in tabular and graphical form. In addition, a photographic study was made to determine the shape of the individual slugs.

The gas fraction and velocity profiles were analyzed by a modification of the variable-density model to include local slip. Results showed that the distribution of the phases is not important in determining the average phase velocity ratio, and that the average slip is a result of local buoyant forces. The photographic study showed that the structure of mercury-nitrogen flow is much different from air-water flow. The slugs are asymmetric, with the gas rising up one wall and the mercury flowing down the opposite wall. This is a result of the high-surface energy of the mercury and, consequently, non-wetting of the wall. Because of the dissimilarity of flow structures, the correlations derived for air-water flow are not applicable to mercury-nitrogen flow.

I. INTRODUCTION

When a liquid and a gaseous phase flow cocurrently through a vertical pipe, the phases distribute themselves in one of several flow patterns depending upon the volumetric flow rate of each phase, and the interphase and intraphase forces. When the gas flow rate is small relative to the liquid flow rate, the gas appears as a suspension of small bubbles. The bubbles move more or less independently of each other at velocities which depend upon their size. This regime is called bubble flow. If the gas concentration is increased at constant mean liquid velocity, bubble coalescence

becomes important; eventually, most of the gas is contained in larger bubbles of very nearly the same diameter as the pipe and many diameters long. This regime is called slug flow. As the gas flow rate is further increased, the slug length increases until eventually the slugs touch to fill the core of the pipe with gas. The liquid flows along the wall as an annular film. This regime is called annular flow. Finally, at very high gas flow rates, the liquid is dispersed as a mist in the gas phase. This last regime is called mist flow.

These are the four basic flow patterns.⁽⁴⁴⁾ However, there are transition regions, and many investigators choose to give these names also. This is particularly true of the transition between slug and annular flow. In this case the annulus periodically forms and collapses again into a slug pattern. This regime is frequently called semi-annular flow.

The regimes of bubble flow and slug flow encompass most cases of practical importance. These processes assume importance, for example, in the design of nuclear reactors which are cooled by boiling water, liquid metals, or organic liquids. Although a great deal of research has been devoted to their study, many details of the flow structure remain virtually unknown. An important reason has been the lack of instrumentation capable of precise measurement of local parameters such as gas fraction, phase velocities, and bubble-size distribution.

This study was initiated with the purposes of developing instruments to measure these quantities and to use these instruments to study a two-phase system. Because of the current interest in boiling liquid-metal heat transfer, the system chosen for study was mercury-nitrogen in vertical slug flow.

To summarize, the plan of this report may be stated as follows:

- (1) Review existing two-phase flow theory with emphasis on slug flow.
- (2) Describe an electrical probe which can be used to measure local values of gas fraction, bubble frequency, and bubble size spectra in a two-phase mixture whose continuous phase is an electrical conductor.
- (3) Describe an impact probe which can be used to measure local values of the liquid velocity in dispersed two-phase flow.
- (4) Present results of a study using a mercury-nitrogen system in vertical slug flow.
- (5) Develop an appropriate model based upon these results.

II. REVIEW OF THE LITERATURE

Publication in the field of two-phase flow has been extensive, and several comprehensive literature surveys are available.^(21,32) A number of empirical and semi-empirical models have been proposed as a basis for flow calculations. The more successful of these are reviewed in the following discussion.

Martinelli et al.,⁽³³⁾ proposed the first general correlation for two-phase, two-component pressure drops. The model was extended to describe forced-circulation boiling of water at high pressures by Martinelli and Nelson⁽³⁴⁾ and is probably the most widely used for calculations of pressure drop.

In the Martinelli model, two-phase flow is visualized as having an unchanging flow pattern along the channel length. The phases are assumed to flow in separate, continuous conduits, each satisfying a separate momentum equation. These conditions are satisfied only by two-phase flow regimes in which the phases are both continuous and without radial pressure gradients, i.e., annular flow. However, the model has been correlated with data taken in other flow regimes to about the same degree of error, indicating that the flow regime assumption is not critical.

Considering an element of fluid of length dz in the direction of flow and inclined θ degrees from the horizon, the momentum equations for the phases are

$$dP + \frac{1}{2g} d [\rho_L \bar{U}_L^2] = \left(\frac{dP}{dz} \right)_{LTP} dz - \rho_L \sin \theta dz \quad ; \quad (2.1)$$

$$dP + \frac{1}{\bar{\alpha}g} d [\bar{\alpha} \rho_G \bar{U}_G^2] + \frac{1}{2\bar{\alpha}g} d [(1 - \bar{\alpha}) \rho_L \bar{U}_L^2] = \left(\frac{dP}{dz} \right)_{GTP} dz - \rho_G \sin \theta dz \quad . \quad (2.2)$$

Radial variations of phase velocity and concentration have been neglected in these equations. In general, these quantities are not constant as reported in References 39 and 42.

The assumption of an unchanging flow pattern implies that the static pressure drops of the phases are equal, so that Eqs. (2.1) and (2.2) can be added to give a general momentum equation for the two-phase stream:

$$dP + \frac{1}{g} d [\bar{\alpha} \rho_G \bar{U}_G^2 + (1 - \bar{\alpha}) \rho_L \bar{U}_L^2] = \left(\frac{dP}{dz} \right)_{TP} dz - \rho \sin \theta dz \quad , \quad (2.3)$$

where

$$\rho = (1 - \bar{\alpha}) \rho_L + \bar{\alpha} \rho_G$$

and

$$\left(\frac{dP}{dz}\right)_{TP} = (1 - \bar{\alpha}) \left(\frac{dP}{dz}\right)_{LTP} + \bar{\alpha} \left(\frac{dP}{dz}\right)_{GTP}$$

The frictional pressure drop was described by the usual friction factor equation:

$$\left(\frac{dP}{dz}\right)_{TP} = f_L \frac{\rho_L \bar{U}_L^2}{2g_c D_L}$$

or

(2.4)

$$\left(\frac{dP}{dz}\right)_{TP} = f_G \frac{\rho_G \bar{U}_G^2}{2g_c D_G}$$

where D_L and D_G are the equivalent hydraulic diameters of the liquid and gaseous flow channels, respectively. These are unknown quantities and must be determined empirically. The friction factors for each phase were expressed by an equation of the form

$$f = C/Re^n \quad , \quad (2.5)$$

where the constants C and n depend upon the flow condition of the particular phase, laminar or turbulent.

Equations (2.4) and (2.5) were used to relate the two-phase frictional pressure gradient to the frictional pressure gradient which would exist if only a single phase were flowing at the same flow rate:

$$\left(\frac{dP}{dz}\right)_{TP} = \phi_L^2 \left(\frac{dP}{dz}\right)_L$$

or

(2.6)

$$\left(\frac{dP}{dz}\right)_{TP} = \phi_G^2 \left(\frac{dP}{dz}\right)_G$$

The multipliers ϕ_L^2 and ϕ_G^2 are empirical functions of the dimensionless factor

$$\chi = \left(\frac{\mu_L}{\mu_G} \right)^{0.111} \left(\frac{\rho_G}{\rho_L} \right)^{0.555} \left(\frac{1}{x} - 1 \right) \quad (2.7)$$

In addition, the correlation depends upon the combination of flow conditions in the phases and, as shown by Martinelli and Nelson,⁽³⁴⁾ has an empirical dependence upon pressure.

Martinelli et al.,⁽³³⁾ established the correlation of ϕ versus χ for horizontal, isothermal flow of air and various liquids: water, oils, kerosene, and benzene, at pressures from 18 to 52 psia. Pipe diameters ranged from 0.0586 to 1.017 in., and lengths from 2.34 to 50 ft.

Lockhart and Martinelli⁽³⁰⁾ improved the correlation by using

$$X^2 = \frac{(dP/dz)_L}{(dP/dz)_G} \quad (2.8)$$

as a correlating factor in place of χ . They also extended the correlation to data from inclined tubes with air, oil, and kerosene at atmospheric pressures and room temperatures. The average scatter of the data was 30%.

Martinelli and Nelson⁽³⁴⁾ established the high-pressure correlation by analyzing the data of Davidson et al.,⁽⁷⁾ for forced-circulation boiling at pressures from 500 to 3300 psia. These data were taken from flow in flat-pancake tube coils and a long horizontal tube. Tube diameters ranged from 0.5 to 1.75 in., and lengths from 10.2 to 53.3 ft. No information was given as to the scatter of the data.

In boiling systems, the momentum change of the stream due to changes of vapor concentration must be considered. This is easily handled by integrating the momentum term of Eq. (2.3) over the flow length. Martinelli and Nelson⁽³⁴⁾ assumed a linear relation between x and z , giving

$$\Delta P_a = \frac{W_T^2}{g \rho_L A_P^2} \left[\frac{(1-x)^2}{(1-\bar{\alpha})} + \frac{x^2}{\bar{\alpha}} \frac{\rho_L}{\rho_G} - 1 \right] \quad (2.9)$$

Levy⁽²⁸⁾ obtained an equation from the Martinelli model which can be used to relate the weight gas fraction x to the volume gas fraction $\bar{\alpha}$ by subtracting Eq. (2.1) from (2.2):

$$d \left[\frac{(1-x)^2}{(1-\bar{\alpha})} + \frac{x^2}{\bar{\alpha}} \frac{\rho_L}{\rho_G} - \frac{1}{2} \frac{(1-x)^2}{(1-\bar{\alpha})} \right] = \frac{g \rho_L A_P^2 \bar{\alpha}}{W_T^2} \left[\left(\frac{dP}{dz} \right)_{GTP} - \left(\frac{dP}{dz} \right)_{LTP} + (\rho_L - \rho_G) \sin \theta \right] dz \quad (2.10)$$

Levy assumed that changes in $\bar{\alpha}$, x , and ρ_L/ρ_G are very slow, so that momentum is exchanged between the water and steam phases, and the frictional plus potential pressure change for the liquid phase equals that for the gaseous phase. Mathematically, this corresponds to writing

$$\frac{d}{dz} \left[\frac{(1-x)^2}{(1-\bar{\alpha})} + \frac{x^2}{\bar{\alpha}} \frac{\rho_L}{\rho_G} - \frac{1}{2} \left(\frac{1-x}{1-\bar{\alpha}} \right)^2 \right] = 0 \quad (2.11)$$

which can be solved with the boundary condition that $x = 0$ when $\bar{\alpha} = 0$ to give

$$x = \frac{\bar{\alpha}(1-2\bar{\alpha}) + \bar{\alpha} \left\{ (1-2\bar{\alpha})^2 + \bar{\alpha} \left[2 \frac{\rho_L}{\rho_G} (1-\bar{\alpha})^2 + \bar{\alpha}(1-2\bar{\alpha}) \right] \right\}^{1/2}}{2 \frac{\rho_L}{\rho_G} (1-\bar{\alpha})^2 + \bar{\alpha}(1-2\bar{\alpha})} \quad (2.12)$$

The momentum-exchange theory, Eq. (2.12), was compared with experimental data for forced-convection boiling of water at pressures from 14.7 to 2000 psia. Predicted values of x were from 20 to 40% higher than found experimentally, the smallest errors being at the highest pressures.

These errors are a result of the assumption

$$\left(\frac{dP}{dz} \right)_{GTP} - \rho_G \sin \theta = \left(\frac{dP}{dz} \right)_{LTP} - \rho_L \sin \theta \quad (2.13)$$

It does not seem possible that this relation is satisfied for all θ , that is, the frictional pressure losses of the phases are equal for horizontal flow, but much different for vertical flow.

A number of papers (1, 5, 10, 17, 29) present analytical treatments of annular flow. In each case, the authors assume that annular flow is characterized by a liquid film of uniform thickness and smooth inner surface where the gaseous core contains no entrained liquid and the flow pattern does not change along the tube length. This is a very idealized situation that is probably never realized.

Armand⁽¹⁾ and Levy⁽²⁹⁾, in studies of horizontal flow, assumed further that the liquid velocity profile is given by the one-seventh power law equation, and the two-phase stream is in equilibrium under the action of the wall shear stress and a static pressure difference. The frictional-pressure-gradient equation is

$$\left(\frac{dP}{dz} \right)_{TP} = \left(\frac{dP}{dz} \right)_L \left[0.701 / (1 - \sqrt{\bar{\alpha}})^2 \left(1 + \frac{8}{7} \sqrt{\bar{\alpha}} \right)^{7/4} \right] \quad (2.14)$$

This theoretical approach predicts values of pressure drop about 20% lower than experiment. These discrepancies can be attributed to the idealized flow geometry.

Calvert and Williams⁽⁵⁾ derived an equation for the momentum flux in the liquid film:

$$\tau = \left[\frac{dP}{dz} - \rho_G \right] \left(\frac{R - \delta}{2} \right) + \left[\frac{dP}{dz} - \rho_L \right] (\delta - y) \quad , \quad (2.15)$$

where (dP/dz) is the static pressure gradient, δ is the film thickness, and y is the variable distance from the wall. Since $\delta \ll R$ and $(dP/dz) \ll \rho_L$, the equation can be simplified to give:

$$\tau = \left[\frac{dP}{dz} - \rho_G \right] \frac{R}{2} - \rho_L (\delta - y) \quad . \quad (2.16)$$

Calvert assumed the film flow was turbulent and used Prandtl's mixing-length theory to determine the liquid velocity profile. In his studies of downward flow of liquid films, Dukler⁽¹⁰⁾ used Deissler's relationship for flow near the wall and Von Karman's equation for flow away from the wall. Dukler's approach is more suitable, since flow in the film near the wall must certainly be laminar. Hewitt⁽¹⁷⁾ extended Dukler's analysis to upward annular flow. Deissler's equation is

$$\tau/\tau_0 = 1 + 0.01 u^+ y^+ \left[1 - \exp(-0.01 u^+ y^+) \right] du^+ dy^+ \quad , \quad (2.17)$$

where

$$u^+ = U_L (\tau_0 / \rho_L)^{1/2}$$

$$y^+ = (\tau_0 / \rho_L)^{1/2} (y \rho_L / \mu_L) \quad .$$

Von Karman's equation is

$$\tau/\tau_0 = (0.36)^2 \left[(du^+/dy^+)^4 / (d^2u^+/dy^{+2})^2 \right] \quad . \quad (2.18)$$

Equation (2.16) may be rewritten in terms of dimensionless variables as

$$\tau/\tau_0 = 1 + y^+(\sigma^3/\eta) \quad , \quad (2.19)$$

where

$$\sigma^3 = \delta^3 / [(\eta^2 \mu_L^2) / (\rho_L^2 g)]$$

and

$$\eta = (\tau_0/\rho_L)^{1/2} (\delta\rho_L/\mu_L)$$

Deissler's expression cannot be solved analytically, and a numerical solution has to be obtained. Von Karman's equation can be integrated to give

$$u^+ - u_i^+ = \frac{1}{2(0.36)} \left[\log\left(\frac{y^+}{y_i^+}\right) + \log\left(\frac{s-1}{s_i-1}\right) + \log\left(\frac{s+1}{s_i+1}\right) + 2(s-s_i) \right] \quad (2.20)$$

where

$$s = \left(1 + \frac{y^+ \sigma^3}{\eta}\right)^{1/2}$$

and

$$s_i = \left(1 + \frac{y_i^+ \sigma^3}{\eta}\right)^{1/2}$$

Hewitt⁽¹⁷⁾ gives tables of numerical solutions of Eqs. (2.17) and (2.20).

Annular flow, as defined in the above analyses, is a very idealized situation which is probably never realized in practice. Measurements of film thickness^(24,35) in horizontal flow show that gravity effects are important. The film can be two or three times as thick at the bottom of the tube as at the top. In both horizontal and vertical flow, surface waves exist which are of approximately the same height as the mean film thickness.⁽²⁷⁾ Liquid entrainment always exists and its effects are usually significant. Armand,⁽¹⁾ Krasiakova,⁽²⁴⁾ and Wicks and Dukler⁽⁴⁶⁾ have measured entrainment concentration in horizontal flow. Armand concluded the liquid mist was uniformly distributed. Hewitt,⁽²⁷⁾ on the other hand, in studies of vertical flow found the entrainment concentration varied both radially and axially.

A review of the literature related to annular flow is given by Lacey et al.⁽²⁷⁾

Bankoff⁽³⁾ treated the bubble flow regime as a suspension of bubbles in the liquid, with bubble concentration gradients existing radially. The bubble concentration is maximum at the center of the pipe, decreases monotonically in a radial direction, and vanishes at the wall. A basic concept introduced is that the gas and liquid have the same velocity at any radial position. The cross-sectional average velocity of the gas is greater than

that of the liquid because the gas is concentrated in the regions of higher velocity. The two-phase mixture is considered to be a single fluid whose density varies radially.

Bankoff showed, by a simplified analysis of the forces on a two-dimensional bubble, that the gas distribution function can be approximated by a power-law function of the radial position. A power-law distribution was assumed for velocity also:

$$U^* = S^{1/n} \quad ; \quad (2.21)$$

$$\alpha^* = S^{1/p} \quad . \quad (2.22)$$

The liquid and gas mass velocities are given by

$$W_L = 2\pi R^2 \rho_L U_m \int_0^1 (1-S)(1-\alpha_m \alpha^*) U^* dS \quad (2.23)$$

and

$$W_G = 2\pi R^2 \rho_G U_m \int_0^1 (1-S) \alpha_m \alpha^* U^* dS \quad , \quad (2.24)$$

and the average gas fraction is given by

$$\bar{\alpha} = 2\alpha_m \int_0^1 \alpha^* (1-S) dS \quad . \quad (2.25)$$

The quality is defined as

$$x = W_G / (W_L + W_G) \quad . \quad (2.26)$$

Three constants are defined in terms of the exponents n and p :

$$\Omega_p = 2p^2 / (1+p)(1+2p) \quad ; \quad (2.27)$$

$$\Omega_n = 2n^2 / (1+n)(1+2n) \quad ; \quad (2.28)$$

and

$$\Omega_{np} = 2(np)^2 / (n+p+np)(n+p+2np) \quad . \quad (2.29)$$

Substituting Eqs. (2.21) and (2.22) into Eqs. (2.23), (2.24), and (2.25) gives

$$W_L = \pi R^2 \rho_L U_m [\Omega_n - \alpha_m \Omega_{np}] \quad ; \quad (2.30)$$

$$W_G = \pi R^2 \rho_G U_m [\alpha_m \Omega_{np}] \quad ; \quad (2.31)$$

and

$$\bar{\alpha} = \alpha_m \Omega_p \quad . \quad (2.32)$$

Substitution into Eq. (2.26) gives

$$\frac{1}{x} = 1 - \frac{\rho_L}{\rho_G} \left[1 - \frac{K}{\bar{\alpha}} \right] \quad , \quad (2.33)$$

where

$$K = (\Omega_n \Omega_p) / \Omega_{np} \quad .$$

A simple expression for the ratio of the average phase velocities can be obtained directly from Eqs. (2.30) and (2.31):

$$\eta = \frac{\bar{U}_G}{\bar{U}_L} = \frac{1 - \bar{\alpha}}{K - \bar{\alpha}} \quad . \quad (2.34)$$

By introducing the gas volumetric flow fraction, defined as

$$\beta = (W_G / \rho_G) / [(W_G / \rho_G) + (W_L / \rho_L)] \quad , \quad (2.35)$$

it can be shown through the use of Eqs. (2.30) and (2.31) that

$$\bar{\alpha} = K \beta \quad . \quad (2.36)$$

Zuber⁽⁴⁷⁾ first derived this relationship between the parameter K and the ratio $\bar{\alpha}/\beta$. Armand^(1,2) observed that in the regimes of horizontal bubble and stratified flow ($\beta < 0.9$), the relation between $\bar{\alpha}$ and β was essentially linear:

$$\bar{\alpha} = C \beta \quad , \quad (2.37)$$

where C depends only upon pressure. The empirical pressure dependence was

$$C = 0.833 + 0.05 \log P \quad , \quad (2.38)$$

where P is pressure in kg/cm^2 .

An expression relating the two-phase frictional pressure gradient to the single-phase liquid pressure gradient was obtained by using a friction factor equation for each gradient and by eliminating the friction factors with the Blasius formula. The two-phase equations were written in terms of the cross-sectional average velocity and density of the mixture. The pressure gradient equation is

$$\frac{(dP/dz)_{TP}}{(dP/dz)_L} = \left(\frac{\bar{\rho}}{\rho_L}\right)^{3/4} \left(\frac{\bar{U}}{\bar{U}_L}\right)^{7/4} \left(\frac{\bar{\mu}}{\bar{\mu}_L}\right)^{1/4} \quad (2.39)$$

An expression for the density ratio was obtained from the definition of the cross-section average density:

$$\frac{\bar{\rho}}{\rho_L} = 1 - \bar{\alpha} \left(1 - \frac{\rho_G}{\rho_L}\right) \quad (2.40)$$

If the condition that the mass flow rates must be equal in the two-phase and the single-phase systems be used, the ratio of the velocities is

$$\frac{\bar{U}}{U_L} = 1 - x \left(1 - \frac{\rho_L}{\rho_G}\right) \quad (2.41)$$

The viscosity ratio is not so easy to describe. Bankoff showed that the ratio may be greater or less than unity, depending upon the bubble size distribution, and, since it enters only as the one-fourth power, it may be taken as unity.

Experimental measurements of phase and velocity distributions are not available; therefore, experimentally determined values of the average gas fraction and quality were used with Eq. (2.33) to calculate values of K which best fit the data. These data were taken for forced-circulation boiling of water at pressures from 14.7 to 2000 psia. The pressure dependence of K found in this way was given by the linear equation

$$K = 0.71 + 0.001 P \quad (2.42)$$

where P is pressure in psia. Equation (2.42) predicts smaller values of K (15% at atmospheric pressure) than Eq. (2.38). In general, Eq. (2.33), with the proper value of K, fell within the scatter of the data. However, K appears to have a dependence on quality. In comparing Eq. (2.39) with pressure drop data at 1000 psia, agreement was good at low qualities, but deviated as the quality increased. This again indicated a quality dependence.

Hughmark(20) extended the variable-density model to two-component flow. Equation (2.33) was used to calculate values of K from data for both horizontal and vertical flow of air and various liquids: water, oil, kerosene, and benzene. These values of K were correlated, by the method of least squares, to a Reynolds number, Froude number, Weber number, and the volumetric liquid flow fraction $(1 - \beta)$. These parameters were suggested by Bankoff. The Weber number was not significant, and K was represented by the three remaining variables in the form

$$Z = \frac{(\text{Re})^{1/6} (\text{Fr})^{1/8}}{(1 - \beta)^{1/4}} \quad (2.43)$$

The first important contributions to the theory of slug flow were the papers of Dumetrescu(11) and of Davies and Taylor,(8) in which they considered the problem: "How fast will a closed tube full of liquid drain when the bottom is removed?" or, alternatively, "How fast will the air column rise in a vertical tube with a closed top when the bottom is opened?" In this case, the fluid will flow freely around the outside of the bubble and down the surface of the tube. The bubble has no lower surface, so the problems associated with the bubble wake are eliminated.

If the vertex of the bubble is taken as the origin of the coordinate system and z the distance below this, then, relatively, the whole system will have a downward velocity U_B . Assuming potential flow and symmetry about the axis of the tube, the governing equations expressed in terms of the velocity potential ϕ and the stream function ψ are

$$\begin{aligned} \frac{\partial^2 \phi}{\partial z^2} + \frac{1}{r} \frac{\partial}{\partial r} \left[r \frac{\partial \phi}{\partial r} \right] &= 0 \quad ; \\ \frac{\partial^2 \psi}{\partial z^2} + \frac{1}{r} \frac{\partial}{\partial r} \left[-r \frac{\partial \psi}{\partial r} \right] &= 0 \quad . \end{aligned} \quad (2.44)$$

The boundary conditions which must be satisfied are:

- (1) constant pressure at the bubble surface: $U_L^2 = 2gz$;
- (2) the origin is a stagnation point;
- (3) a uniform bubble velocity, U_B , for large negative values of z ;
- (4) zero radial velocity at the wall.

Particular solutions to Eq. (2.44) which satisfy boundary conditions (3) and (4) are

$$\phi = -U_B z + \sum_n A_n \exp[K_n(z/R)] J_0\left(K_n \frac{r}{R}\right) \quad (2.45)$$

and

$$\psi = -\frac{1}{2} U_B r^2 + r \sum_n A_n \exp[K_n(z/R)] J_1 K_n \frac{r}{R} \quad , \quad (2.46)$$

where K_n is a root of the equation: $J_1(s) = 0$. Boundary conditions (1) and (2) must still be satisfied, and an explicit solution seems unlikely.

Davies and Taylor⁽⁸⁾ obtained a rough approximation to the flow near the top of the air column by using only one term of the series Eqs. (2.45) and (2.46). Dumetrescu⁽¹¹⁾ made a similar approximation but carried the series to the third term. His results gave

$$U_B = 0.495 \sqrt{gR} \quad . \quad (2.47)$$

Agreement with experimental measurements was remarkably good for large tubes (of $\frac{3}{4}$ - and 1-in. diameters), but the theory tends to over-estimate the velocity for small tubes ($\frac{1}{2}$ -in. diameter). This is attributed to viscosity effects at low Reynolds numbers. Griffith and Wallis⁽¹⁶⁾ measured the rise velocity of infinite slugs; their results agree with Eq. (2.47).

The flow of finite slugs is characterized by large bubbles, almost filling the tube, separated by slugs of liquid. The nose of the bubble is round and the tail is nearly flat. Because of the problem of describing the flow in the bubble wake, a mathematical analysis of slug flow is a formidable problem, and its description must rely heavily upon experiment.

Laird and Chisholm⁽²⁵⁾ studied the pressure and forces along cylindrical bubbles in vertical flow, noting their velocities, by admitting bubbles singly into the bottom of a vertical column 38 ft long and of 2-in. ID. The column was filled with stagnant water. The observed velocities ranged from 0.76 to 0.88 ft/sec for slugs 4 in. to 50 in. long. This is in close agreement with the value of 0.81 ft/sec predicted by Dumetrescu's analysis for an infinite slug.⁽¹¹⁾ Apparently the effect of the wake upon bubble velocity is unimportant. This conclusion is supported by later work of Griffith and Wallis.⁽¹⁶⁾ The analysis of Dumetrescu and that of Davies and Taylor describes adequately the flow of finite slugs in stagnant liquid. Laird and Chisholm also concluded that the pressure drop over most of the bubble length is zero and the shear force at the wall is proportional to the 1.5th power of the bubble length.

Griffith and Wallis⁽¹⁶⁾ also studied the effect of an imposed liquid velocity upon the slug velocity. They used an 18-ft vertical test section equipped for admitting water at either the top or bottom. Three tube sizes were used: 1-in., $\frac{3}{4}$ -in., and $\frac{1}{2}$ -in. inside diameter. The relative slug

velocity was observed to increase as the water velocity increased. In an attempt to rationalize these results, a constant, C_2 , was defined in terms of Dumetrescu's equation as

$$C_2 = U_B / (0.495 \sqrt{gR}) \quad , \quad (2.48)$$

where C_2 is an empirical function of the Reynolds number based upon the liquid velocity, and the Reynolds number based upon the slug velocity. In general, the correlation showed that C_2 varied directly with Reynolds number based upon the liquid velocity, and inversely with Reynolds number based upon the slug velocity. In the limit as both Reynolds numbers became very large, $C_2 = 1.0$.

The variation of C_2 was explained as resulting from the oncoming liquid velocity profile as "seen" by the bubble. For example, in the case of upflow, the profile is distorted in the direction necessary to pass the bubble; hence, a higher rise velocity would be expected.

In slug flow studies, Griffith and Wallis⁽¹⁶⁾ observed that as the distance between two slugs became smaller than some critical value, the trailing slug, influenced by the wake of the leading slug, rose faster. Eventually, the two slugs agglomerated. This characteristic process of developing slug flow was the subject of a paper by Moissis and Griffith.⁽³⁶⁾ Since the shape of the velocity profile of the liquid behind the leading bubble was believed to be most important, the approach to the problem was to determine the velocity profile, analytically and experimentally, and to measure the rise velocity of the trailing slug in the liquid having a specified velocity profile.

If the intersection of the centerline with the plane of the trailing edge of the slug is taken as the origin of the coordinate system and z as the distance below this, then, relatively, the whole system will have a downward velocity U_B . The problem is then one of a jet entering a circular pipe through an annular orifice while the pipe is moving in the same direction as the jet. However, the pipe velocity is not equal to the jet velocity.

Moissis assumed the flow to be steady with no wall friction, and the core mixing process to be faster than the boundary-layer growth at the wall. He used Reichardt's inductive theory of turbulence⁽¹⁸⁾ to obtain a mathematical expression for the velocity profiles. Reichardt's theory is based upon experimental data for free turbulent flow, such as a free jet in an infinite fluid. This annular jet is enclosed and the tube walls are so close that they must certainly have an effect.

The Reichardt equation of motion was written in terms of dimensionless variables as

$$\frac{\partial M}{\partial z^*} - \frac{4\Lambda}{D_p r^*} \frac{\partial}{\partial r^*} r^* \frac{\partial M}{\partial r^*} = 0 \quad , \quad (2.49)$$

where

$$r^* = \text{radius} = 2r/D_p \quad ;$$

$$z^* = \text{length} = z/D_p \quad ;$$

$$M = \text{momentum flux} = (m - m_\infty)/(m_c - m_a) \quad .$$

The local momentum flux is $m = P + \rho U_L^2$, and m_c and m_a are the momentum fluxes evaluated at $z^* = 0$. The term m_∞ is evaluated as $z^* \rightarrow \infty$. Equation (2.49) was solved with the following boundary conditions:

$$\begin{aligned} r^* = 0 & \quad dM/dr^* = 0 & \quad (\text{symmetry}) \\ r^* = 1 & \quad dM/dr^* = 0 & \quad (\text{no wall friction}) \\ z^* = 0 & \quad M = m_c & \quad 0 < r^* < d/D_p \\ & \quad M = m_a & \quad d/D_p < r^* < 1 \end{aligned}$$

to give

$$M = \sum_n \frac{2(d/D_p) J_1[K_n(d/D_p)]}{K_n J_0^2(K_n)} J_0(K_n r^*) \exp[-\int (4K_n^2 \Lambda / D_p) dz^*] \quad . \quad (2.50)$$

Velocity profiles were measured in the wake of a stationary plastic slug in a 2-in. tube in which the water flow was downward. The slug dimensions were $1\frac{3}{4}$ in. in diameter by 6 in. long. The total pressure was measured with a pitot tube; static pressure was measured at the wall. The data obtained were used to calculate values of the momentum transfer length from Eq. (2.50). These values were expressed by the equation

$$\Lambda = \frac{(1.07)^2 z}{2[1 + 100z/D_p]} \quad . \quad (2.51)$$

The rise velocity of the trailing slug was determined from motion pictures taken of two consecutive slugs as they rose in the tube. The scope of the film studies included tube diameters ranging from $\frac{1}{2}$ to 2 in. The data were correlated with the empirical equation

$$U_B/U_\infty = 1 - 8 \exp[-1.06 L_s/D_p] \quad , \quad (2.52)$$

where U_B is the trailing bubble velocity; U_∞ is velocity of the lead slug; and L_s is the separation distance. In general, the results showed that wake effects are important for a length of about seven tube diameters.

III. A MODIFICATION OF THE VARIABLE-DENSITY MODEL TO INCLUDE LOCAL SLIP

In the variable-density model,⁽³⁾ the local phase velocities are assumed to be equal:

$$U_L = U_G$$

The model can be extended to include local slip by making the less restrictive assumption that the local phase velocity ratio is independent of radial position. This implies that

$$U_L^* = U_G^*$$

where

$$U_L^* = U_L / U_{Lm}$$

and

$$U_G^* = U_G / U_{Gm}$$

The local phase velocity ratio is given by

$$\Phi = U_{Gm} / U_{Lm}$$

where U_{Lm} and U_{Gm} are the maximum liquid and gas velocities, respectively, at the center of the tube.

Assuming power law distributions for both velocities and gas fraction,

$$U_L^* = U_G^* = S^{1/n} \tag{3.1}$$

and

$$\alpha^* = S^{1/p} \tag{3.2}$$

where

$$\alpha^* = \alpha / \alpha_m$$

The exponents n and p are positive constants.

Then

$$W_L = 2\pi R^2 \rho_L U_{Lm} \int_0^1 (1-S)(1-\alpha_m \alpha^*) U_L^* dS \quad (3.3)$$

and

$$W_G = 2\pi R^2 \rho_G U_{Gm} \int_0^1 (1-S) \alpha_m \alpha^* U_G^* dS \quad , \quad (3.4)$$

and the average gas fraction is given by

$$\bar{\alpha} = 2\alpha_m \int_0^1 (1-S) \alpha^* dS \quad . \quad (3.5)$$

With the use of Eqs. (3.1) and (3.2) and the constants defined by Eqs. (2.27), (2.28), and (2.29), the integrals give

$$W_L = \pi R^2 \rho_L U_{Lm} (\Omega_n - \alpha_m \Omega_{np}) \quad ; \quad (3.6)$$

$$W_G = \pi R^2 \rho_G U_{Gm} (\alpha_m \Omega_{np}) \quad ; \quad (3.7)$$

$$\bar{\alpha} = \alpha_m \Omega_p \quad . \quad (3.8)$$

The cross-section average phase velocities follow from Eqs. (3.6) and (3.7):

$$\bar{U}_L / U_{Lm} = (\Omega_n - \alpha_m \Omega_{np}) / (1 - \alpha_m \Omega_p) \quad ; \quad (3.9)$$

$$\bar{U}_G / U_{Gm} = \Omega_{np} / \Omega_p \quad . \quad (3.10)$$

The mass fraction of gaseous phase is defined as

$$x = W_G / (W_G + W_L) \quad . \quad (3.11)$$

Substitution of Eqs. (3.6), (3.7), and (3.8) into Eq. (3.11) gives

$$\frac{1}{x} = 1 - \frac{\rho_L}{\rho_G} \frac{1}{\Phi} \left[1 - \frac{K}{\bar{\alpha}} \right] \quad , \quad (3.12)$$

where

$$K = \Omega_n \Omega_p / \Omega_{np}$$

is a constant. Equation (3.12) is identical with Eq. (2.33) when $\Phi = 1$.

A simple expression for the average slip velocity ratio is obtained from Eqs. (3.9) and (3.10):

$$\eta = \frac{\bar{U}_G}{\bar{U}_L} = \Phi \left(\frac{1 - \bar{\alpha}}{K - \bar{\alpha}} \right) \quad , \quad (3.13)$$

which is to be compared with Eq. (2.34). Equation (3.13) shows the average phase velocity ratio is the product of two slip factors, one due to local slip, Φ , and the other due to nonuniform phase distribution.

IV. EXPERIMENTAL APPARATUS

A. Flow System

The flow system employed is shown schematically in Fig. 1. It is a natural-circulation loop in which metered streams of mercury and nitrogen are fed to a mixer. The resulting two-phase mixture flows through the test section into a separator. The nitrogen exhausts to a vent, and the mercury returns by gravity flow to the mixing section.

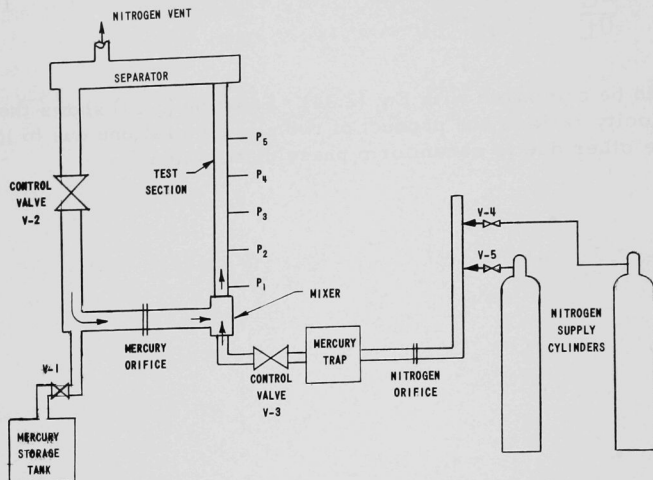


Fig. 1. Mercury-Nitrogen Flow System

Stainless steel pipe, Schedule 40, was used throughout, and all threaded joints were sealed with a resin-base paint.

1. Components

a. Mercury-Nitrogen Mixer

The mercury-nitrogen mixer (see Fig. 2) was constructed from a pipe tee. The nitrogen entered at the bottom, and the mercury entered at the side. Upon leaving the mixer, the two-phase stream passed through a 150-mesh screen which was intended to give a uniform gas distribution and bubble size at the entrance to the test section. A similar mixer was used by Richardson.⁽⁴⁰⁾

b. Test Section

Two test sections were constructed: one for use with the electric probe and one for use with the impact probe. Each test section

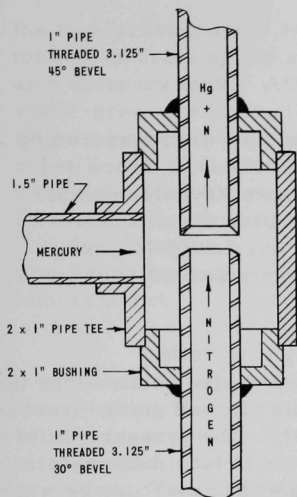


Fig. 2. Mercury-Nitrogen Mixer

comprised a 60-in. length of 1-in. pipe, with probe and static pressure taps welded at 90° to each other. Figure 3 shows the test section used with the electric probe. The other test section was similar except that the probe taps were located 1.25 in. lower, at the same level as the static pressure taps.

c. Separator

The separator was a 42-in. length of 4-in. Lucite tube. The velocity of the two-phase stream entering at one end decreased, due to the increase in cross-sectional area, allowing the gas to escape to an outside vent while the mercury entered the 1.5-in. downcomer.

d. Mercury Storage Tank

The mercury was stored in a tank constructed from a 1-ft length of 10-in. pipe (see Fig. 4).

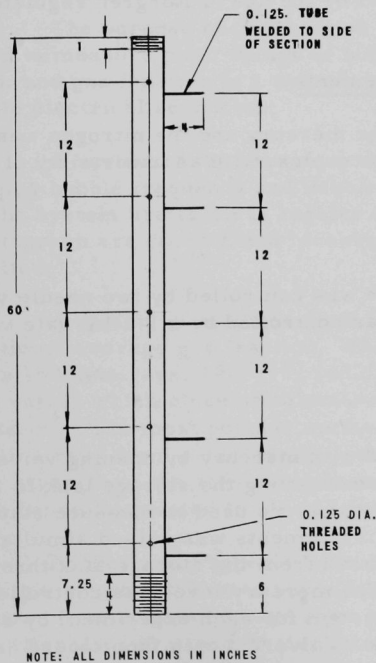


Fig. 3. Test Section

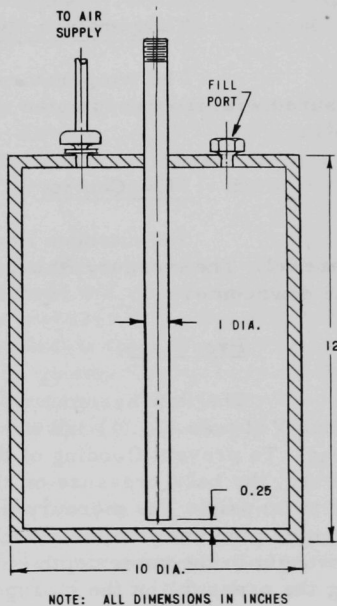


Fig. 4. Mercury Storage Tank

2. Instrumentation and Control

a. Orifice Meters

The nitrogen and mercury flow rates were measured by means of orifice meters built according to specifications of Grace and Lapple.⁽¹⁴⁾ Calibration curves over the approximate Reynolds number range were known with an uncertainty of 0.5%. Orifice diameters were 0.0312 in. and 0.0625 in. for nitrogen, and 0.2500 in., 0.5000 in., and 1.0000 in. for mercury. In each case, the uncertainty was ± 0.0005 in.

b. Pressure Measurements

The static pressure was measured at five points along the test section by means of regular stand tubes. This allowed static-pressure measurements with a maximum error of 0.1 in. Hg. The pressure differential across the orifice meters was measured with U-tube manometers containing water for nitrogen flow, and containing either mercury or water for mercury flow.

The mercury-storage tank pressure and the nitrogen pressure were regulated and measured by the use of Norgren regulators and pressure gages.

c. Temperature Measurements

The temperature of the mercury and the nitrogen was measured with iron-constantan thermocouples, with an uncertainty of $\pm 0.5^\circ\text{C}$.

d. Flow Control

The nitrogen flow rate was controlled by two needle valves in parallel. The mercury flow rate was controlled by a 1.5-in. gate valve in the downcomer.

3. Procedure

The flow system was filled with mercury by opening valves V-1 and V-2 (see Fig. 1) and slowly pressurizing the storage tank to 50 psig. To prevent flooding of the manometers used to measure static pressure, the back pressure on these instruments was raised simultaneously to 30 psig. The mercury was forced from the storage tank through the center pipe and into the system. The mercury level was controlled and brought to the same depth in the system for each experiment by regulating the pressure on the storage tank. Valve V-1 was then closed and

the tank pressure was released. (This arrangement also afforded a method of draining the system rapidly in the event of an emergency, such as a mercury leak.) After the system was filled with mercury and the static-pressure lines cleared of bubbles, the gas flow was started by setting the pressure regulators on the storage cylinders at 50 psig, opening valve V-4 or V-5 wide and V-3 a small amount. Valve V-3 was regulated until the nitrogen flow was about 0.25 cfm. The nitrogen was allowed to flow until the mercury temperature was constant. Initially, both the mercury and nitrogen were at room temperature. However, because of friction, the temperature of the mercury rose several degrees above room temperature.

After the system had "warmed up," the nitrogen and the mercury flow was adjusted to the desired values with valves V-2 and V-3 and the following flow variables were recorded: static pressure gradient, back pressure on the manometers, nitrogen and mercury temperatures, nitrogen and mercury orifice manometer readings, and the barometric pressure. These variables were checked frequently, usually at 5-min intervals, during the course of each experiment (~1.5 hr).

B. Electric Probe

The purpose of this section is to describe a probe which can be used to measure point values of bubble frequency, bubble-size distribution, and gas fraction in a two-phase system. The continuous phase must be an electrical conductor.

A review of the literature reveals only one technique for determining bubble frequency and bubble-size distributions.*⁽¹⁵⁾ Photographs of the system are taken at regular intervals, and the bubbles in each photograph are counted and measured. Such a technique is obviously limited.

A variety of methods have been used for determining the cross-sectional average gas fraction. These include the attenuation of gamma rays and beta rays;^(38,39,19) radioactive tracers;⁽⁹⁾ photography;⁽¹⁵⁾ and valves which close simultaneously to isolate the test section contents.⁽²²⁾ The most popular method is the gamma-ray technique, wherein gamma rays from a radioactive source are passed through the stream. The strength of the attenuated beam is a function of the stream density and, hence, is related to the gas fraction.

Hooker and Popper⁽¹⁹⁾ have studied the gamma-attenuation method at some length and have made a detailed uncertainty analysis. In one series of tests, gamma rays from a Tm¹⁷⁰ source were beamed through and attenuated by steam-water mixtures contained in a 2.5-in., rectangular

*A number of devices have been used for counting single bubbles.^(4,13,37)

test section. The emergent radiation was detected by a scintillation crystal-photomultiplier tube assembly. Their analysis showed that the uncertainty increases as the gas fraction decreases, ranging from $\pm 2.9\%$ for a gas fraction of 1.0, to $\pm 7.5\%$ for a gas fraction of 0.10. Similar tests were made with three idealized preferential phase distributions simulated in Lucite. It was concluded that the gamma-ray technique was unsatisfactory for nonhomogeneous flow. Cook⁽⁶⁾ and Egen⁽¹²⁾ reported errors as large as 93% in annular flow.

The gamma-ray technique was improved by Petrick.⁽³⁹⁾ He used a traversing method in which the source and detector were moved across the channel to get a gas-fraction profile. The cross-sectional average gas fraction was obtained by integration of this profile. The difference between the gas fractions measured by gamma attenuation and the known gas fraction for simulated preferential gas distributions was 7.3% for the traversing technique, whereas that of the "one shot" method was 36.5%. However, for homogeneous gas distributions the errors were similar, being about 1.5%.

The gamma-ray method is reasonably accurate for determining cross-sectional average gas fractions when the gas is uniformly distributed, the test section offers a radiation path greater than 1 in. of water, and the gas fraction is greater than about 0.25. These conditions are not met frequently.

The beta-ray attenuation method has the advantage of higher sensitivity, since the beta rays are absorbed more readily than are gamma rays and, hence, can be used with accuracy at very low gas fractions. On the other hand, because of their low energy, beta rays can penetrate only short distances, and a limit is placed upon the size of channel used.

An analysis of the beta-ray technique was made by Perkins.⁽³⁸⁾ In this work, beta rays from a Y^{90} source were beamed through a 0.19-in.-thick annular space containing a boiling liquid. Various organic liquids as well as water were used in the subcooled and the saturated boiling state. The error analysis showed that for homogeneous gas distributions an accuracy of 0.5% can be obtained, whereas for local boiling of water an uncertainty of 0.001 in. may be expected in the vapor thickness. Due to an unknown preferential phase distribution, the beta-ray method is subject to the same errors as the gamma-ray method.

The tracer technique employs a radioactive salt dissolved in the liquid phase. The assumption is made that the salt does not appear in the gas phase and, hence, the count is proportional to the liquid fraction. This technique is subject to the same errors as the gamma-ray method, particularly those due to preferential phase distribution. Further, the tracer salts adhere to the walls of the apparatus so that the resulting background noise must be considered when the signal is analyzed.

Dengler,⁽⁹⁾ using $\text{Mn}^{52}\text{Cl}_2$ at a concentration of 40 mc/liter in a 1-in. vertical tube, calculated the maximum error in his experiments to be 16%, with the majority of data within 10%.

The use of photographs to determine bubble volumes and, subsequently, gas fractions is limited to simple systems of few bubbles and to transparent, rectangular channels.

All of the foregoing techniques detect space-averaged rather than local values of the gas fraction and give no information on individual bubble frequencies and size distributions. In general, the phases are not distributed uniformly in the pipe cross section. In vertical flow, the gas tends to concentrate near the pipe axis due to the unbalanced drag force on an individual bubble in the presence of the wall. Because of the higher concentration of gas at the center of the pipe, the bubbles tend to be larger there than near the wall.

It is clear that for further progress in understanding the two-phase flow mechanism, local values of the flow variables must be measured.

1. Definition of Variables

Bubble frequency and bubble-size distribution at a point are, respectively, the number of bubbles that pass the point per unit time, and the frequency with which bubbles of various diameters pass the point. Thus, the bubble frequency is

$$f = N/T \quad ,$$

where f is the frequency in bubbles/second, and N is the total number of bubbles that pass the probe in time T .

The bubble-size distribution is expressed in terms of a cumulative bubble distribution function:

$$B(\xi) = \int_0^{\xi} b(\xi) d\xi \quad . \quad (4.1)$$

The function $B(\xi)$ is the probability that the diameter of an observed bubble will be less than ξ . Thus,

$$B(a) = P(\xi < a) \quad . \quad (4.2)$$

The probability that a bubble diameter fall in an interval $a < \xi < b$ is

$$P(a < \xi < b) = B(b) - B(a) \quad . \quad (4.3)$$

Further, the density function can be obtained by differentiating $B(\zeta)$:

$$b(\zeta) = \frac{d}{d\zeta} B(\zeta) \quad (4.4)$$

In slug flow, the gas slug-length and liquid slug-length distributions are also important quantities, and cumulative distribution functions are defined analogously to Eq. (4.1). For gas slugs,

$$G(\zeta) = \int_1^{\zeta} g(\zeta) d\zeta \quad , \quad (4.5)$$

and for liquid slugs,

$$L(\zeta) = \int_0^{\zeta} l(\zeta) d\zeta \quad . \quad (4.6)$$

Remarks about the significance of the bubble distribution function are also valid for these functions. The lower limits of the integrals in Eqs. (4.5) and (4.6) are different, since a gas slug is defined as a bubble for which $\zeta \geq 1$, whereas a liquid slug is defined as the liquid which separates two gas slugs and, hence, has no minimum size. In general, the liquid slug is not homogeneous, but contains many small ($\zeta < 1$) gas bubbles.

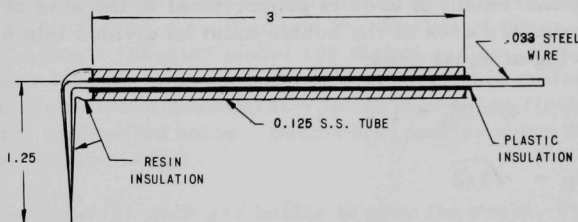
In general, the point, or local void fraction is defined for any two-phase flow field as the probability that gas will exist at the point under consideration. For flow with stationary time-averaged properties (quasi-steady flow), this probability is the fraction of time that gas exists at the point. The sample interval must be large compared with the time scale of the flow oscillations, $1/f$, where f is the local bubble frequency. On the other hand, it must be small compared with any slow variations in the field of flow that are not to be associated with the instantaneous fluctuations. When the flow has stationary space-averaged properties (homogeneous flow field), the probability is the fraction of a spherical volume, surrounding the point, occupied by gas. When the flow is neither quasi-steady nor homogeneous, averaging in either time or space coordinates is inappropriate. An ensemble average at the point in time and space must be taken over a large number of experiments with the same initial and boundary conditions. For quasi-steady flow, the gas fraction is therefore expressed as

$$\alpha = \frac{1}{T} \int_0^T [1 - f(t)] dt \quad , \quad (4.7)$$

where α is the void fraction, and $f(t)$ is a discontinuous function of time with a value of unity when liquid exists at the point, and zero when gas exists at the point. The time interval T must satisfy the conditions stated above.

2. Method

The electric probe consists of a 6-in. length of 0.033-in. steel wire with a 1.25-in. steel sewing needle welded at 90° to the end (see Fig. 5). The steel wire is encased in a 3-in. length of 0.125-in. stainless steel tube. The needle is insulated electrically from the tube except for the point by a resin varnish. The probe is oriented with the needle pointing into the flow. A 1.5-v battery and 10,000-ohm resistor are connected in series with the probe to ground. The conducting liquid is also grounded.



NOTE: ALL DIMENSIONS IN INCHES

Fig. 5. Electric Probe

The principle of operation is the instantaneous measurement of local resistivity in the two-phase mixture. When the needle tip is in contact with liquid, the circuit is closed; when it is in contact with gas, the circuit is open. Since the series resistance is large compared to the probe resistance (10,000:1), the voltage drop across the series resistance will form a square wave of irregular frequency and constant amplitude of 1.5 v (see Fig. 6).

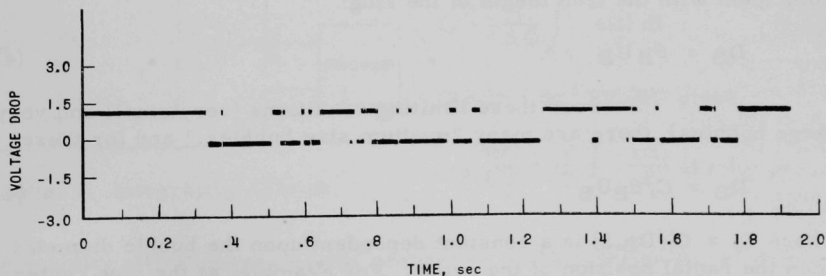


Fig. 6. Photographic Record of Electric Probe Signal

Three important characteristics of the phase distribution can be determined from an analysis of the signal:

(1) the frequency with which the phase changes at the probe tip, which may be identified with the local bubble frequency;

(2) the dwell time of each gas bubble. A statistical analysis can be used to relate this quantity to the bubble diameter as follows. If it is assumed that the bubbles are spherical, that they are not deflected by the probe, and that they are small compared with the pipe diameter, then the bubble motion is random, and the probe has an equal probability of piercing any segment of projected area. The average diameter pierced is that diameter which divides the projected bubble area into two parts, the probability of piercing each part being equal. Since the probability of piercing any increment of area is proportional to the size of the increment, the projected area of the bubble must be divided into a circle and an annular ring of equal area.

$$\pi\epsilon^2/r = 4/\pi D_B^4 = 1/2 \quad ;$$

$$\epsilon/D_B = \sqrt{1/2} \quad , \quad (4.8)$$

where ϵ is the diameter of the circular area and, from symmetry, also the average bubble diameter pierced. It is related to the dwell time θ_B by the bubble velocity U_B :

$$\epsilon = \theta_B U_B \quad . \quad (4.9)$$

Hence, it follows that

$$D_B = \sqrt{2} \theta_B U_B \quad . \quad (4.10)$$

For very large bubbles (slugs), the measured length is coincident with the true length of the slug:

$$D_B = \theta_B U_B \quad . \quad (4.11)$$

Between these limiting conditions (very small and very large bubbles), there are many "medium size bubbles," and for these

$$D_B = C_1 \theta_B U_B \quad , \quad (4.12)$$

where $C_1 = C_1(D_B, S)$ is a constant dependent upon the bubble diameter and upon the radial position of the probe. For example, at the pipe center ($S = 1$), $\sqrt{2} \geq C_1 \geq 1$, as bubble size varies from very small to very large, whereas at the wall ($S = 0$), $\infty \geq C_1 \geq 1$, as bubble size varies from small to large.

The problem is very complicated, and an approximation must be made. The dependence upon the radial position of the probe is ignored, and it is assumed that limiting values of $\sqrt{2}$ are to be taken for bubbles of zero diameter, and of 1 for slugs. Further, it is assumed that the dependence of C_1 upon bubble diameter is linear. The effect of these approximations will be to increase the apparent frequency of small bubbles near the wall. However, this is not a serious limitation in this study, since the regime of flow is principally slug flow.

(3) the fraction of time that the circuit is open. This may be identified with the local gas fraction.

3. Signal Analysis

An attempt was made to measure bubble frequency by means of a flip-flop circuit. The circuit counts the number of times the voltage drops to zero, using a "Shasta" Model 100 digital scaler. The response of the circuit was adequate to count a 100-cps square-wave voltage correctly, but the bubble counts were considerably lower than those from the photographic record, as detailed below. Bubble frequencies were therefore obtained by the latter method.

The time for each gas bubble to pass the probe, θ_B , was determined by measuring the lengths from a photographic record of the signal. A "Visicorder" Model 906 was used to record the signal. This is a high-speed recorder capable of recording signal frequencies up to 2000 cps. The record is made visible by exposure to fluorescent light.

The fraction of time the circuit was closed was determined by electronically integrating the signal for a time T . The integrating circuit is shown schematically in Fig. 7. This is a standard circuit for which the following relationship holds:

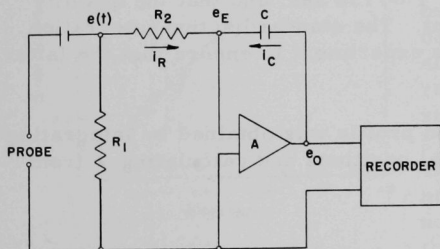


Fig. 7. Integrating Circuit

$$e_0 = -\frac{1}{RC} \int_0^T e(t) dt \quad (4.13)$$

Division by $-ET/RC$ gives

$$-e_0 \frac{RC}{ET} = \frac{1}{T} \int_0^T \frac{e(t)}{E} dt = (1-\alpha) \quad (4.14)$$

The quantity $e(t)/E$ possesses the properties of the function $f(t)$ as defined by Eq. (4.7).

The integrating circuit had two principal components: an amplifier with power supply, and a recorder. The amplifier was a Philbrick Model UPA-2 with an output voltage range of ± 115 v and a gain of 10^7 . The power supply was a Philbrick Model R100B compound regulated, dual supply with rated output at ± 300 v. A Bristol Model 1PH560 strip recorder with 100-mv range was used to record the output signal. The circuit time constant, $RC = 2$ sec, allowed integration for as long as 150 sec.

4. Procedure

The probe was held in position by a "Swedglock" tube fitting modified by replacing the first farrow with a 0.125-in. "O" ring and reversing the second farrow. This allowed the probe to be moved in or out and still be leak proof. The axial orientation of the needle was effected by aligning a dial pointer attached to the probe at 180° to the needle with an etched vertical line centered on the test section. The lateral position of the probe was determined by measuring the distance between the test section and the vertical pointer.

A photographic record of the probe signal was obtained by feeding the signal to one channel of the photographic recorder. The recorder was started and allowed to run for 120 sec. This corresponded to a 50-ft trace of the signal.

Before the gas flow was started, when the system was full of mercury, the steady probe signal was integrated for a time $T = 150$ sec. From Eq. (4.13) this output signal is simply ET/RC and is the quantity by which all succeeding output signals are divided to get the liquid fraction, Eq. (4.14). This technique does not require an exact value of the integration constant RC . However, it does require that each succeeding integration be made over the same interval, $T = 150$ sec, and that the quantity ET/RC be constant for the experiment. The standardization integration was performed again at the end of the experiment to ensure that the latter prevailed.

The complete gas-fraction profile was obtained by integrating the probe signal at each of eight radial positions and calculating α from Eq. (4.14) with the constant ET/RC .

5. Discussion

Since this is the first method capable of measuring point values of gas fraction, there are no previous data with which to compare the results. However, it is possible to check the cross-sectional average value, obtained by integrating the profile, with the average obtained by some other method. One such method employs the measured static-pressure

profile along the pipe. From a consideration of the momentum equation, one finds that changes in the kinetic energy of the stream contribute less than 0.5% to the total static-pressure loss and may be neglected. Similarly, the frictional loss is estimated by the method of Lockhart and Martinelli⁽³⁰⁾ to be less than 2% of the total static-pressure loss and, hence, may be neglected.

The local pressure gradient is therefore very nearly equal to the mean density at that axial position:

$$-dP/dz = \rho \quad , \quad (4.15)$$

where the mixture density is defined by

$$\rho = (1 - \bar{\alpha}) \rho_L + \bar{\alpha} \rho_G \quad . \quad (4.16)$$

If it be noted that $\rho_G/\rho_L \approx 1/4000$, $\bar{\alpha} \rho_G$ may be neglected, and a relation between the pressure gradient and the cross-sectional average gas fraction is obtained:

$$-dP/dz = (1 - \bar{\alpha}) \rho_L \quad . \quad (4.17)$$

Values of α may be calculated from the measured pressure gradient along the test section. Figure 8 shows the comparison of $\bar{\alpha}$ determined in this manner with values obtained by integrating the α profiles. The agreement is excellent, the maximum deviation being 0.06.

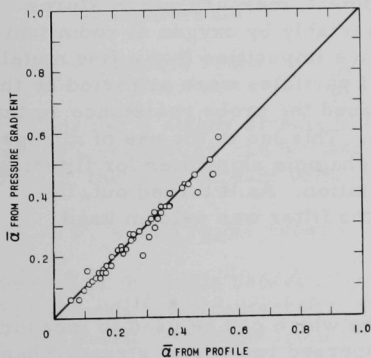


Fig. 8. Average Gas Fraction from Integration of Profile and from Measured Pressure Gradient

The sources of error inherent in the method were analyzed to determine the uncertainty limits. The electronics circuits were examined by replacing the probe signal with a standard half-square wave signal from a function generator. The integration circuit was capable of integrating signals of 1200 cps with a maximum error no greater than the error of reading the recorded signal from the strip chart, i.e., the output signal was accurate to ± 0.2 v. Since two readings of the chart were required for each

value of the gas fraction determined and the full chart range was used, the uncertainty in the gas fraction value was less than ± 0.004 .

The response of the photographic recorder was fast enough to record the dwell time of every bubble which the probe pierced. The diameter of the probe tip was about 0.02 in., and bubbles in this range of size are probably deflected. However, because of the limit of chart speed, bubbles of $\theta_B = 0.003$ sec or smaller appeared in the record as square waves of width $\frac{1}{64}$ in. or less. The method of measuring these widths was not accurate enough to differentiate between bubbles of this size, and they were all given a $\theta_B = 0.003$. The wave width for larger bubbles was measured to the nearest $\frac{1}{64}$ in., and the individual dwell times were accurate to $\theta_B \pm 0.003$ sec.

The digital scaler error was 1% for the range of frequencies from 1 to 100 cps. The range of values was from 1 to 20 cps.

The radial position of the probe could be measured to the nearest $\frac{1}{32}$ in. or about 3% of the test section diameter.

The method is applicable to any gas-liquid or liquid-liquid system in which the continuous phase is an electrical conductor. It is particularly advantageous for systems in which the continuous phase is a liquid metal, because of: (1) high conductivity and low capacitance; (2) high surface energy resulting in non-wetting of the probe, so a fast break in the circuit is obtained; and (3) high density which allows the liquid metal to remain continuous at high rates of gas flow.

In the early stages of development, mercury-air mixtures were used. Mercury is not oxidized appreciably by oxygen at room temperature; however, there were enough trace impurities that a fine metal oxide powder was produced. These small particles were attracted by the electrically positive needle tip and increased the probe resistance so that the measurements were not reproducible. This led to the use of nitrogen instead of air and to the installation of a chamois skin filter for filtering the mercury after each day of experimentation. As it turned out, the nitrogen eliminated oxide formation and the filter was seldom used.

C. Impact Probe

In this section is described a probe which can be used to measure point values of the liquid velocity in a dispersed two-phase stream when the gas fraction distribution is known.

Krasiakova(24) used a pitot tube to measure stagnation pressures in stratified and annular horizontal flow, with the static pressure measured at the wall. These results gave the liquid and the gas velocity distributions as well as the thickness of liquid film. However, no attempts were made to measure velocities in dispersed flow.

Armand⁽¹⁾ used a knife edge to cut the exit two-phase stream from a pipe into two parts. The amount of gas and liquid flowing on each side of the blade was measured. The mass flow distribution of each phase was calculated by differentiating the results as the knife was moved across the channel. In other experiments, the exit stream was cut into an annular ring and a circle by tubes of different diameters. The radial distribution of each phase was calculated by differentiating the results as the differences in the tube diameters were varied. The first of these methods was used by Griffith and Wallis⁽¹⁶⁾ in studies of a two-phase boiling analogy.

These methods are adequate for application to exit streams. However, they are inconvenient to use and the results are subject to errors of graphical differentiation. It would be convenient to have a method of determining local values of velocity at any point in the test section. Such a technique is described below.

1. Method

The impact probe (see Fig. 9) consisted of a 3-in. length of 0.125-in. stainless steel tube with one end plugged and the other end equipped with a tube adapter. At $\frac{3}{64}$ in. from the plugged end, a $\frac{1}{32}$ -in. hole was drilled in the tube wall. The probe was held in position, with the small hole pointing into the flow, by a traversing mechanism similar to the one used for the electric probe.

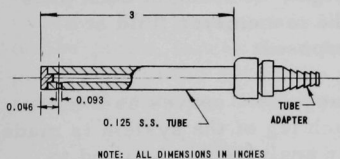


Fig. 9. Impact Probe

Consider a steady stream of a single fluid as it flows around the probe. Newton's second law can be used to relate the impulse pressure upon the probe to the local stream velocity, with the result

$$P_i = \rho(U^2/g_c)(1 - \cos \theta) \quad (4.18)$$

where θ is the angle between the axis of the pipe and the direction of the fluid directly after contact with the probe. This angle is assumed to be 90° and small deviations from this will be taken into account by the probe calibration.

In a steady two-phase system, as slugs of gas and liquid alternately pass the probe, the impulse pressure fluctuates between the limits $\rho_G(U_G^2/g_c)$ for gas and $\rho_L(U_L^2/g_c)$ for liquid. The value for gas is very small compared to that for the liquid and may be taken as zero. This is particularly true for the case of mercury-nitrogen flow in which

$$(\rho_G U_G^2)/(\rho_L U_L^2) \approx 1/400$$

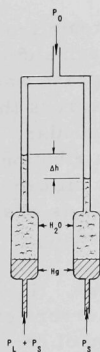


Fig. 10

Schematic of Differential Pressure-Measuring System

Using this approximation, the instantaneous impulse pressure acting upon the probe can be written

$$P(t) = \rho_L(U_L^2/g)f(t) \quad , \quad (4.19)$$

where $f(t)$ is a discontinuous function of time. The function takes the value unity when liquid exists at the probe, and zero when gas exists at the probe.

A static-pressure measurement was taken at the pipe wall and the two signals fed to a differential manometer system (see Fig. 10). The pressure signals were fed through 0.125-in., clear plastic pressure tubing to the bottom of two baffle-filled capacitance tanks. These tanks were constructed of 12-in. lengths of 3-in., Schedule 80, stainless steel pipe, with each end capped. The capped ends were equipped with tube adapters, and the tanks interconnected with a tube line and valve. Each tank was filled about one-third with mercury and the remainder with water. A Merriam Model A282 manometer was mounted above the capacitance tanks to measure differences in fluid height. A constant back pressure at the top of the manometer maintained the manometer fluid at a convenient level. The system serves three purposes:

(1) The water-over-mercury arrangement serves as a mechanical amplifier. The volume of water in each leg of the system is made equal and maintained constant, so a manometer analysis can be used to relate the differential manometer reading to the pressure it represents. Doing this gives

$$\Delta P = \Delta h [(d_2/d_1)^2 (\rho_m - \rho_w) + \rho_w] \quad , \quad (4.20)$$

where Δh is the differential manometer reading; d_1 is the inside diameter (2.90 in.) of the capacitance tank; and d_2 is the inside diameter (0.25 in.) of the manometer tube. The bracketed term is the effective manometer fluid density ρ_F . For this system at 23°C, $\rho_F = 68.2 \text{ lb/ft}^3$.

(2) The baffle tanks and the flow-line resistance damp the flow oscillations so a time-smoothed manometer reading is obtained. A relation between this reading and the local liquid velocity results when Eq. (4.19) is time smoothed;

$$\overline{\Delta P} = \overline{\rho_L(U_L^2/g) f(t)} \quad . \quad (4.21)$$

By assuming the turbulent velocity fluctuations of the liquid are small compared with the liquid velocity per se, U_L is a constant and Eq. (4.21) becomes

$$\overline{\Delta P} = \rho_L(U_L^2/g) \overline{f(t)}$$

or

$$\overline{\Delta P} = \rho_L (U_L^2 / g) (1 - \alpha) \quad , \quad (4.22)$$

since

$$\bar{f}(t) = (1 - \alpha)$$

by Eq. (4.7).

Equation (4.22) can be solved for U_L to give

$$U_L = C_p \{ (g \rho_F \Delta h) / [\rho_L (1 - \alpha)] \}^{1/2} \quad , \quad (4.23)$$

where an empirical calibration constant, C_p , and $\overline{\Delta P} = \rho_F \Delta h$ have been introduced.

(3) The constant pressure at the top of the manometer automatically keeps gas from entering the probe. If the manometer is at equilibrium so that it does not drift up or down over a long period of time, then as gas passes the probe the impulse pressure drops to zero. The constant back pressure in the manometer, being larger than the pressure on the probe, forces the mercury to flow from the probe. When mercury passes the probe again, the probe pressure is greater than the back pressure and mercury flows into the probe. The flow is small in both cases because of the large line resistance and the small pressure difference (1 or 2 in. Hg).

Table I

CALIBRATION OF IMPACT PROBE

| \bar{U}_{orifice} , ft/sec | \bar{U}_{probe} , ft/sec | $\frac{\bar{U}_{\text{orifice}}}{\bar{U}_{\text{probe}}} = C_p$ |
|--|--------------------------------------|---|
| 1.42 | 1.44 | 0.986 |
| 1.48 | 1.48 | 1.000 |
| 1.56 | 1.59 | 0.980 |
| 1.68 | 1.71 | 0.983 |
| 1.78 | 1.78 | 1.000 |
| 1.89 | 2.01 | 0.940 |
| 1.94 | 1.98 | 0.980 |
| 2.02 | 2.02 | 1.000 |
| 2.10 | 2.15 | 0.976 |
| 2.19 | 2.21 | 0.990 |
| 2.22 | 2.25 | 0.988 |
| 2.33 | 2.42 | 0.963 |
| 2.42 | 2.56 | 0.945 |
| 2.43 | 2.60 | 0.935 |
| 2.92 | 3.02 | 0.966 |
| Average C_p : 0.974 | | |

2. Calibration

The impact probe was calibrated by integrating the velocity profiles to get an average liquid velocity and comparing this with the average velocity determined from knowledge of the total mass flow rate and the average gas fraction. Table I shows these velocities with values of the calibration constant, $\bar{U}_{\text{orifice}}/\bar{U}_{\text{probe}}$. The average value is 0.974 and the mean error is 3%.

3. Procedure

The back pressure at the top of the manometers was increased

to a value slightly greater than the static pressure in the test section. Then the pressure lines connecting the probe and static tap and manometer system were opened, and mercury was forced slowly from the probe into the test section. In this way, the manometers approached a stable reading from above, and gas was prevented from entering the probe. When the manometer reached a steady difference, the value was recorded and the probe was moved to a new radial position. This procedure was continued until the complete profile was obtained. The probe was always started at the center, $S = 1$, and moved closer to the wall with each succeeding measurement. In this way, the pressure differential was usually decreasing and it was never necessary for mercury to be drawn into the manometer lines from the test section. The resistance lines and the capacitance of the system were very large and, hence, the response of the system was very slow. For this reason, about 5 min were required between measurements for the system to reach a stable reading.

4. Discussion

In developing the probe, the principal problem was to prevent gas from entering the probe. Initially, a pitot tube was used, and the pressure signal was measured by means of a Statham Model PM80TC pressure transducer. This is a zero volume-displacement instrument; once it is filled, it is unnecessary for additional liquid to be drawn from the system. It was thought that by having a constant-volume measuring system there would be no opportunity for gas to enter the lines. However, as gas passed the pitot tube, mercury drained from the vertical section of the pitot tube, leaving it filled with nitrogen. For this reason, the impact probe described above was adopted.

The impact probe gave inconsistent results. Apparently, after a few minutes of operation, the mercury would drain from the horizontal probe, leaving it full of nitrogen. The transducer was replaced by the manometer system described above. This worked very well.

The probe is applicable to any gas-liquid or liquid-liquid system in which one phase is much more dense than the other. For this reason, it worked very well for mercury-nitrogen flow, but would be less valuable for most liquid-liquid systems or for steam-water flow at higher pressures.

V. RESULTS AND DISCUSSIONS

The inertial, viscous, gravitational, and surface forces, as well as the phase concentrations, determine which flow pattern will exist in two-phase flow; hence, the Reynolds, Froude, and Weber numbers are, in general, important correlating factors. These numbers are defined as

$$\text{Re} = \frac{\text{Inertial Force}}{\text{Viscous Force}} = \frac{\rho V^2 / g_c}{\mu V / g_c L} \quad ; \quad (5.1)$$

$$\text{Fr} = \frac{\text{Inertial Force}}{\text{Gravitational Force}} = \frac{\rho V^2 / g_c}{\rho g L / g_c} \quad ; \quad (5.2)$$

$$\text{We} = \frac{\text{Inertial Force}}{\text{Surface Force}} = \frac{\rho V^2 / g_c}{\sigma / L} \quad , \quad (5.3)$$

where ρ is the density; μ the viscosity; σ the surface tension; V the velocity; and L a characteristic length.

The experiments of this study were performed at room temperature, and buoyant and surface forces, which contain only fluid properties, were constant. For this reason, the Froude and Weber numbers may be eliminated as correlating factors and the dependence upon inertial force concentrated in the Reynolds number. Two factors were used to characterize the results: a Reynolds number based upon the total mass flow rate and the liquid viscosity:

$$\text{Re} = 4W_T / \pi D_p \mu_L \quad , \quad (5.4)$$

and the volumetric gas flow fraction β , defined as

$$\beta = Q_G / (Q_L + Q_G) \quad . \quad (5.5)$$

The Reynolds number is much larger than β , so a reduced Reynolds number, defined as

$$\text{Re}^* = \text{Re} \times 10^{-4} \quad , \quad (5.6)$$

was used to simplify presentation of the data.

The variables were correlated with the Re^* and β in the form

$$V = m \text{Re}^{*n} \beta^p \quad , \quad (5.7)$$

where V represents any flow variable, and m , n , and p are constants. A least-squares computer program was used to determine the values of m , n , and p which fit the data best.

A. Gas Fraction and Liquid Velocity Profiles

Profiles of the gas fraction and the liquid velocity were measured at three positions along the length of the test section, measuring from the inlet at $\xi = 5.7, 28.5,$ and 51.5 , where the dimensionless length ξ is given as z/D_p . For many runs, an additional measurement of gas fraction was made at $\xi = 17.1$. In every case, those measurements taken at $\xi = 5.7$ exhibited entrance effects as demonstrated by the changing profiles of both gas fraction and liquid velocity. At $\xi = 28.5$ and 51.5 , the flow was always fully developed, as indicated by stable profiles, static pressure, and bubble-size spectra. The measurements at $\xi = 17.1$ showed entrance effects for small β , and the flow was fully developed for large β .

The data for gas fraction for all experiments are presented in Table A-1, page 62. Figure 11 shows typical gas-fraction profiles at $\xi = 5.7$. Figure 12 shows gas fraction profiles at $\xi = 5.7$ for increasing values of β from 0.13 to 0.52, and decreasing values of Re^* . This illustrates the profile development as the relative volumetric flow rate of gas is increased. The phenomenon of a maximum gas fraction at the wall is a result of the non-wetting character of mercury and, hence, the partial absence of a liquid film at the wall. Slugs of gas and liquid alternately enter the test section. Because of the high surface energy of mercury and the instability of the undersurface of the mercury slug, the gas tends towards the wall, giving a maximum gas fraction. This type of flow is unstable, as evidenced by large fluctuations (1 to 5 in. Hg) of static pressure in the mixer, and a large slip velocity ratio (as high as 10).

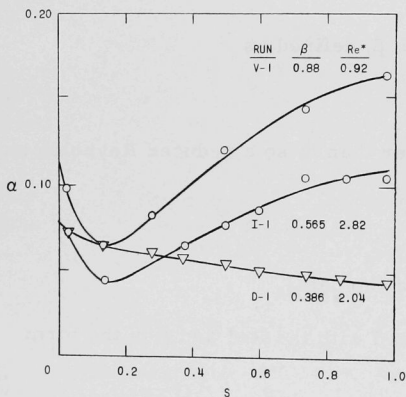


Fig. 11. Typical Gas Fraction Profiles at $\xi = 5.7$

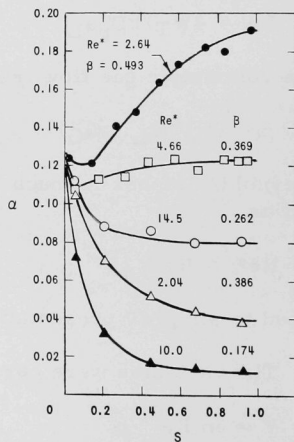


Fig. 12. Developing Gas Fraction Profiles for Increasing Values of β

Further up the tube, at $\xi = 28.5$, the flow becomes stable, and because of frictional forces at the wall, the gas fraction profile is inverted to become dome shaped, with a maximum at the center of the tube. A similar inversion of the gas-fraction profile was reported by Wright⁽⁴²⁾ for forced-convection boiling at a point in the channel which coincided with a change from subcooled to saturated boiling. This change in shape was thought to coincide with a change in flow regime from bubble flow to slug and annular flow. As the flow advances up the column to $\xi = 51.5$, further change in the gas-fraction profile is indistinguishable. Figure 13 shows profiles at $\xi = 28.5$ and $\xi = 51.5$ for a typical experiment. The average gas fraction at $\xi = 51.5$ is larger because of a decrease in static pressure and the consequent expansion of the nitrogen. Figure 14 shows profiles at $\xi = 28.5$ for constant β and varying Re^* .

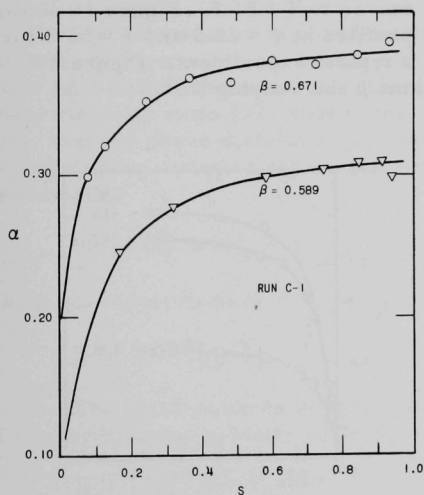


Fig. 13. Gas Fraction Profiles at $\xi = 28.5$ and $\xi = 51.5$ for Varying β and Constant $Re^* = 2.6$

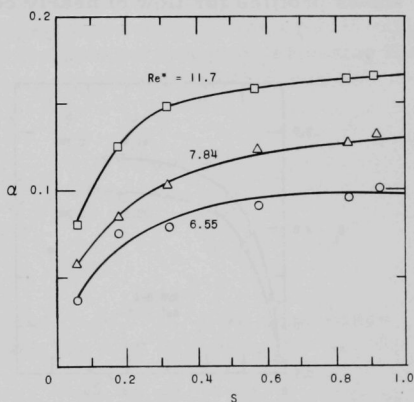


Fig. 14. Gas Fraction Profiles at $\xi = 28.5$ and $\xi = 51.5$ for Varying Re^* and Constant $\beta = 0.3$

The gas-fraction profiles measured at $\xi = 17.1$ were concave downward, usually as those in developed flow, but the static-pressure fluctuations and slip velocity ratio were high enough to indicate only partial flow development. For this reason, these profiles were of less interest and only a few measurements were made.

The data for liquid velocity are presented in Table A-2, page 66. Figure 15 shows typical liquid-velocity profiles at $\xi = 5.7$ for increasing β .

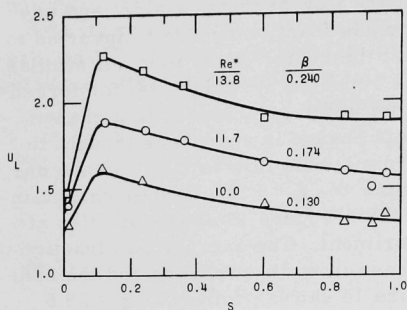


Fig. 15. Liquid Velocity Profiles at $\xi = 5.7$ for Large Re^* and Increasing β

shows profiles for flow of nearly constant β and varying Re^* .

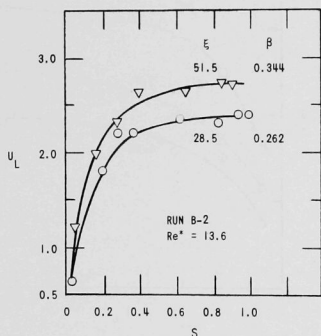


Fig. 16. Liquid Velocity Profiles at $\xi = 28.5$ and $\xi = 51.5$ for Varying β and Constant $Re^* = 13.6$

The maximum liquid velocity occurs near the point of maximum gas fraction but is displaced because of wall friction.

The gas-velocity profile is expected to have approximately the same shape, with a maximum near the wall. The development of the liquid-velocity profiles parallels that of the gas fraction. At $\xi = 28.5$, the profile becomes dome shaped, with a maximum at the tube center. No further change occurs as the flow moves to $\xi = 51.5$. Figure 16 shows profiles at $\xi = 28.5$ and $\xi = 51.5$ for a typical experiment. Figure 17

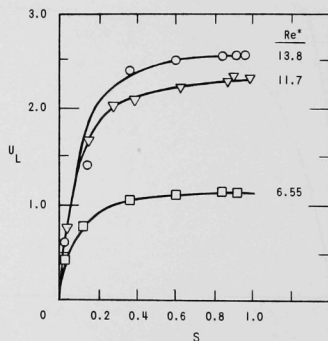


Fig. 17. Liquid Velocity Profiles for $\beta = 0.3$ and Varying Re^*

The profiles, in fully developed flow of both gas fraction and liquid velocity, decrease rapidly near the wall; and, although it is doubtful that the gas fraction goes to zero (because of non-wetting), both profiles can be expressed conveniently as a power function of the radial position S :

$$a^* = S^{1/p}$$

and

$$U_L^* = S^{1/n}$$

The data from Tables A-1 and A-2 were plotted logarithmically, and values of n and p were found by determining the best straight line through the data points. The results are presented in Table A-3, page 66. The magnitudes vary from 7 to 43, indicating very flat profiles, as would be expected for slug flow. In addition, values of the constant

$$K = (\Omega_p \Omega_n) / \Omega_{np}$$

and the contribution to the average slip velocity ratio

$$\lambda = (1 - \bar{\alpha}) / (K - \bar{\alpha}) \quad (5.8)$$

were calculated and are presented. The average phase-velocity ratio determined from the mass flow rate of each phase is also given for comparison.

The importance of phase distribution is maximum when n and p take their respective minimum values (~ 7 and ~ 7) and $K = 0.98$. The maximum value of λ calculated was 1.02. Comparison of this value with the average phase-velocity ratio (> 2) shows, for the system of mercury-nitrogen in slug flow, that the phase distribution is relatively unimportant in determining the average phase-velocity ratio. For practical purposes, plug flow can be assumed:

$$\alpha^* = U_L^* = U_G^* = 1 \quad ,$$

which corresponds to $K = 1$, and

$$\Phi = \eta = \bar{U}_G / \bar{U}_L \quad .$$

The least-squares program was used to determine the dependence of the local phase-velocity ratio $\Phi(=\eta)$, upon the flow variables Re^* and β :

$$\Phi = 0.74 / \beta^{0.5} (Re^*)^{0.7} \quad . \quad (5.9)$$

The error in this correlation is $\pm 10\%$.

When the profiles are very flat, as they are here, an error of 30% or 50% in the exponent is almost indistinguishable in the shape of the profile; and so it is difficult to determine the influence of the flow variables, Re^* and β , upon the values of n and p . In general, the values of n and p have approximately the same magnitude and vary in the same direction; that is, when p increases, n increases. The least-square program was used to determine the variation of n and p with Re^* and β . These results give

$$n = 32.67(\beta/Re^*)^{0.32} \quad ; \quad (5.10)$$

$$p = 27.43(\beta/Re^*)^{0.25} \quad . \quad (5.11)$$

The error in these equations is large. However, they give the general variation of the exponents with the correlating factors. These equations show that the more gas present, the more uniform is the distribution of both the gas fraction and liquid velocity; and as the total mass flow rate, which is essentially the mass flow rate of mercury, increases, the gas tends to become more concentrated at the tube center.

The parameter $C = \bar{\alpha}/\beta$, from Armand's empirical equation (2.37), was evaluated from the cross-sectional average gas fraction determined by integrating the profiles and the volumetric gas flow fraction. These results are shown in Table A-4, page 67. The average value $C = 0.472$ and the deviations from the mean for each experiment are also shown. For mercury-nitrogen flow, Armand's relation is not valid, since C depends upon the flow variables. The values of C were correlated with an equation of the form

$$C = 0.47 \beta^{0.88} (\text{Re}^*)^{0.41} \quad (5.12)$$

The error in this equation is less than 5%.

B. Average Velocities

Three important average velocities can be defined for two-phase flow: the cross-sectional average velocity of each phase, \bar{U}_L and \bar{U}_G , and the mixture velocity, which is the total volume flow rate divided by the cross-sectional area of the tube:

$$V_{\text{Mix}} = (Q_G + Q_L)/A_p \quad (5.13)$$

The fact that the gas phase flows faster than the liquid phase can be expressed by three different slip velocities. These are:

the gas slip velocity

$$u_G = \bar{U}_G - V_{\text{Mix}} \quad (5.14)$$

the liquid slip velocity

$$u_L = \bar{U}_L - V_{\text{Mix}} \quad (5.15)$$

and the relative slip velocity

$$u_R = u_G - u_L \quad (5.16)$$

The relative slip velocity is most frequently used. Also, many papers present slip data as the average phase-velocity ratio, $\eta = \bar{U}_G/\bar{U}_L$. Values of η are given in Table A-3, page 66.

Values of the three average velocities and the three slip velocities, defined above, are given in Table A-5, page 68, for all experiments and for fully developed flow. The least-squares program was used to correlate the slip velocity terms to the correlating factors β and Re^* . The gas slip velocity and the relative slip velocity were found to be independent of Re^* , but inversely proportional to β as follows:

$$u_G = 0.87 (\beta)^{-0.76} \quad ; \quad (5.17)$$

$$u_R = 1.52 (\beta)^{-0.41} \quad . \quad (5.18)$$

The error in Eq. (5.13) was $\pm 16\%$, and in Eq. (5.14), $\pm 19\%$. The liquid slip velocity was given by:

$$u_L = 1.0 (\beta)^{1.96} (Re^*)^{0.43} \quad . \quad (5.15)$$

The error in this correlation was much greater ($\pm 30\%$) than in Eqs. (5.13) and (5.14). The larger error results from subtracting terms of comparable size and the propagation of their individual errors.

C. Bubble Diameter and Slug Length Spectra

Photographic records of the electrical probe signal were taken at three positions along the length of the test section: $\xi = 5.17, 28.5,$ and 51.5 ; and at three radial positions: $S = 1, 0.5,$ and 0.06 . Graphical representations of the corresponding bubble-size distributions are shown in Figs. 18, 19, and 20. From these results, it may be concluded that the small bubbles are uniformly distributed in the tube cross section. This is undoubtedly due to the turbulence and mixing action of the two-phase flow.

Further observation shows that the probability is 0.8 to 0.9 for any bubble that $\xi < 1$. Nevertheless, by comparison of the total area under the bubble distribution curve to the area under the curve for $\xi < 1$, it can be shown that the contribution of such bubbles to the gas fraction is less than 10%. This is characteristic of slug flow. Despite the greater number of small bubbles, most of the gas flow is carried by slugs. These results are in agreement with photographic studies of air-water flow being carried out at Argonne National Laboratory.

The cumulative gas slug length distribution for fully developed flow is shown in Figs. 21 and 22. The corresponding liquid slug distribution is shown in Fig. 23. Since the length of a slug is its center-line length, it is necessary to take slug-length data only at $S = 1$. The distributions show that, frequently, the distance between gas slugs is small (< 1 in.). Results of air-water flow studies by Griffith and Wallis⁽¹⁶⁾ and by Moissis and Griffith⁽³⁶⁾ indicate that when two slugs approach each other too closely

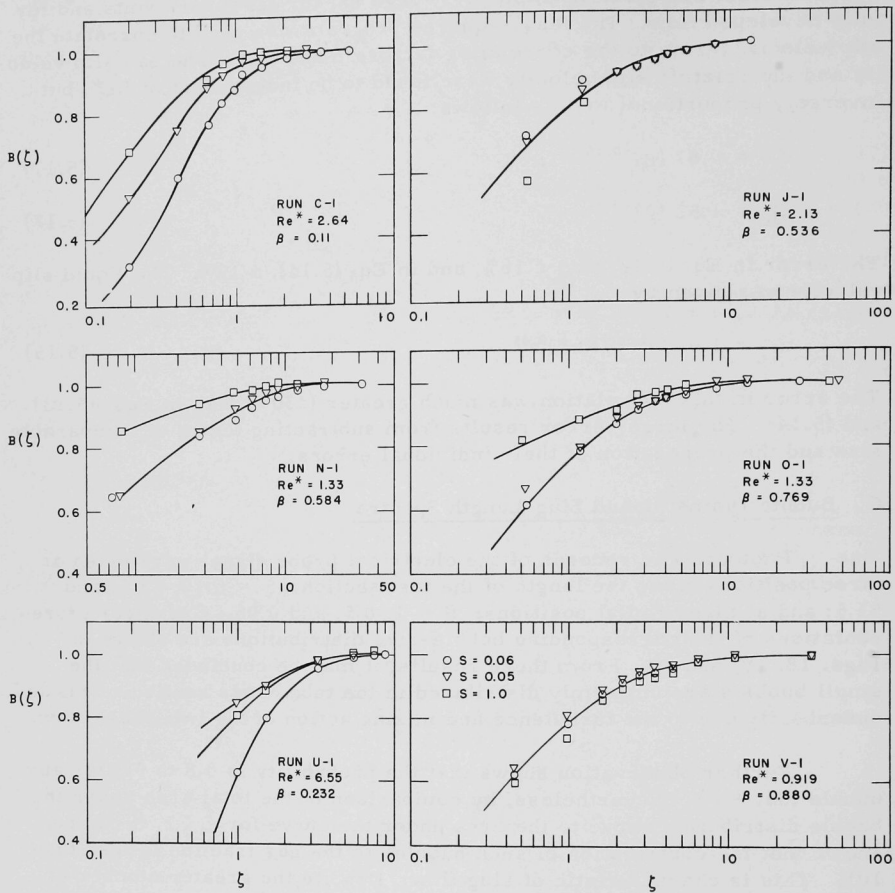


Fig. 18. Bubble Size Distribution at $\xi = 5.7$

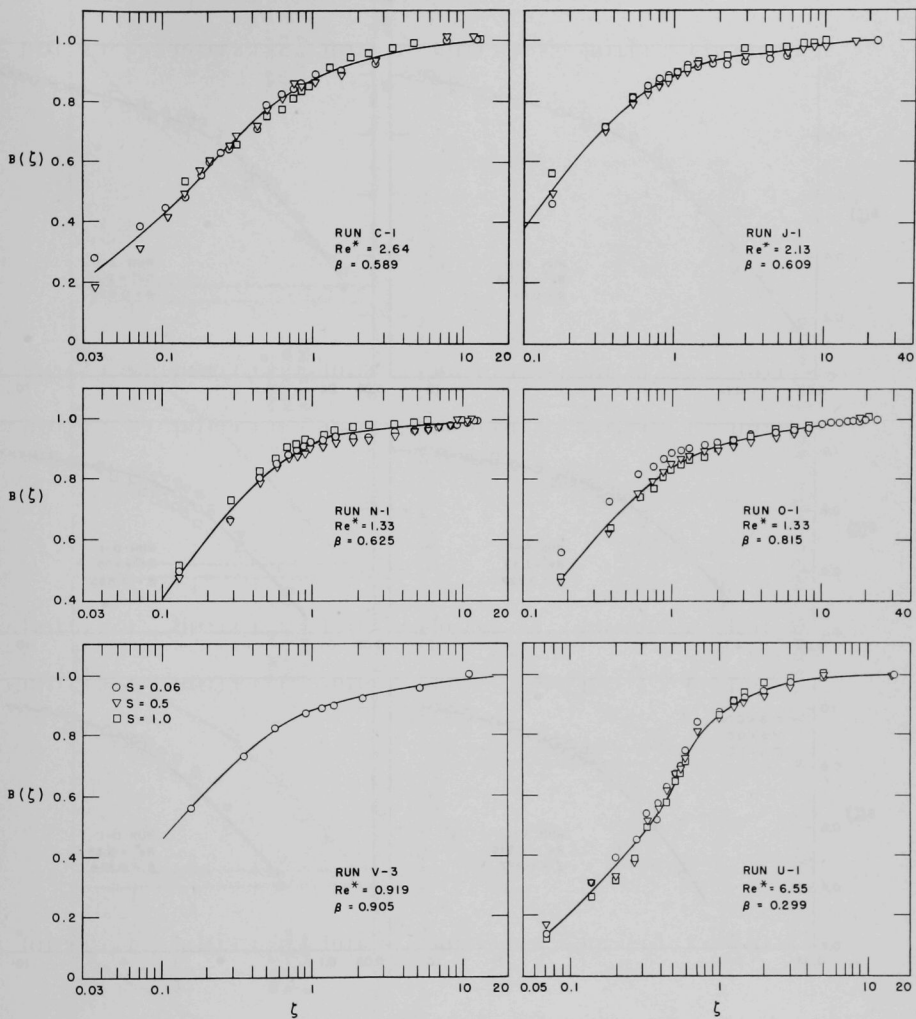


Fig. 19. Bubble Size Distribution at $\xi = 28.5$

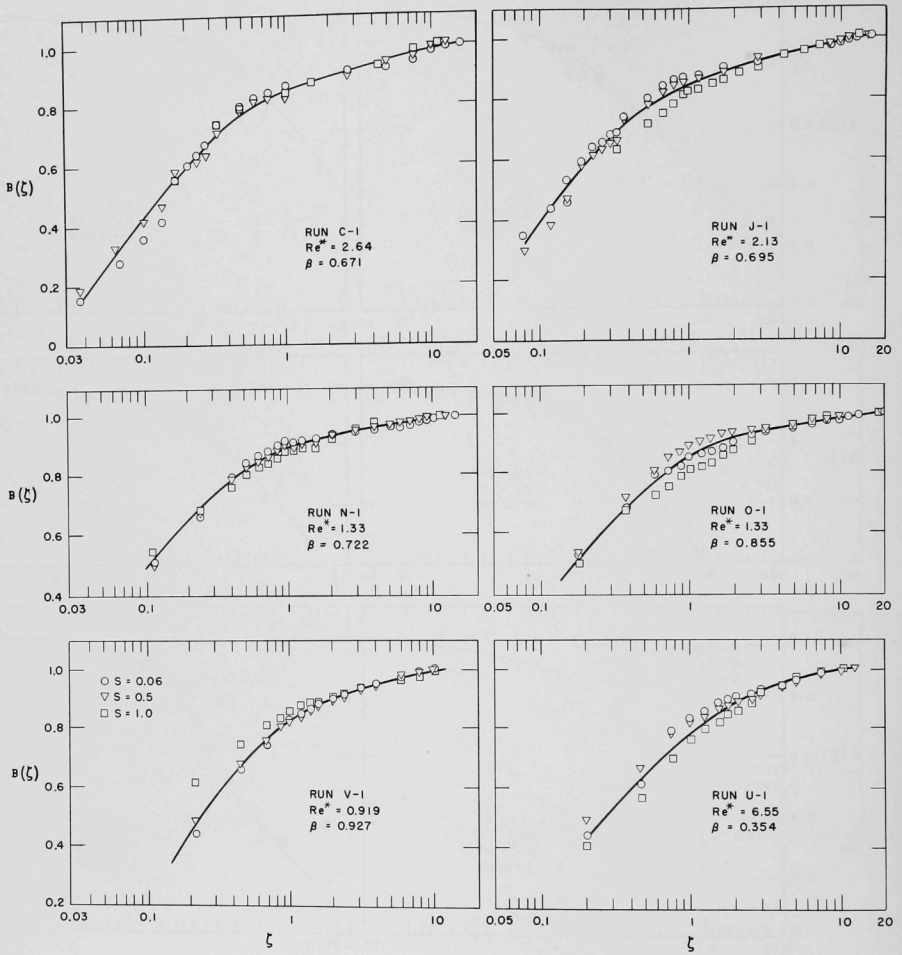


Fig. 20. Bubble Size Distribution at $\xi = 51.5$

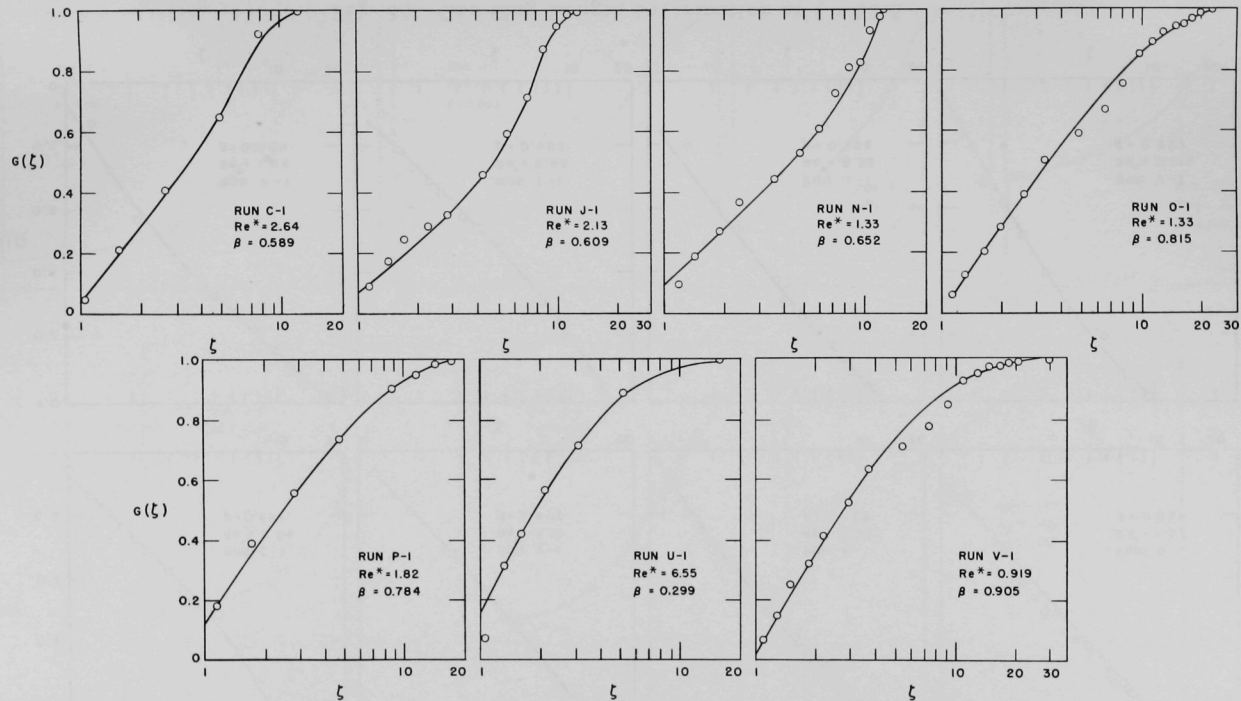


Fig. 21. Gas Slug Length Distribution at $\xi = 28.5$

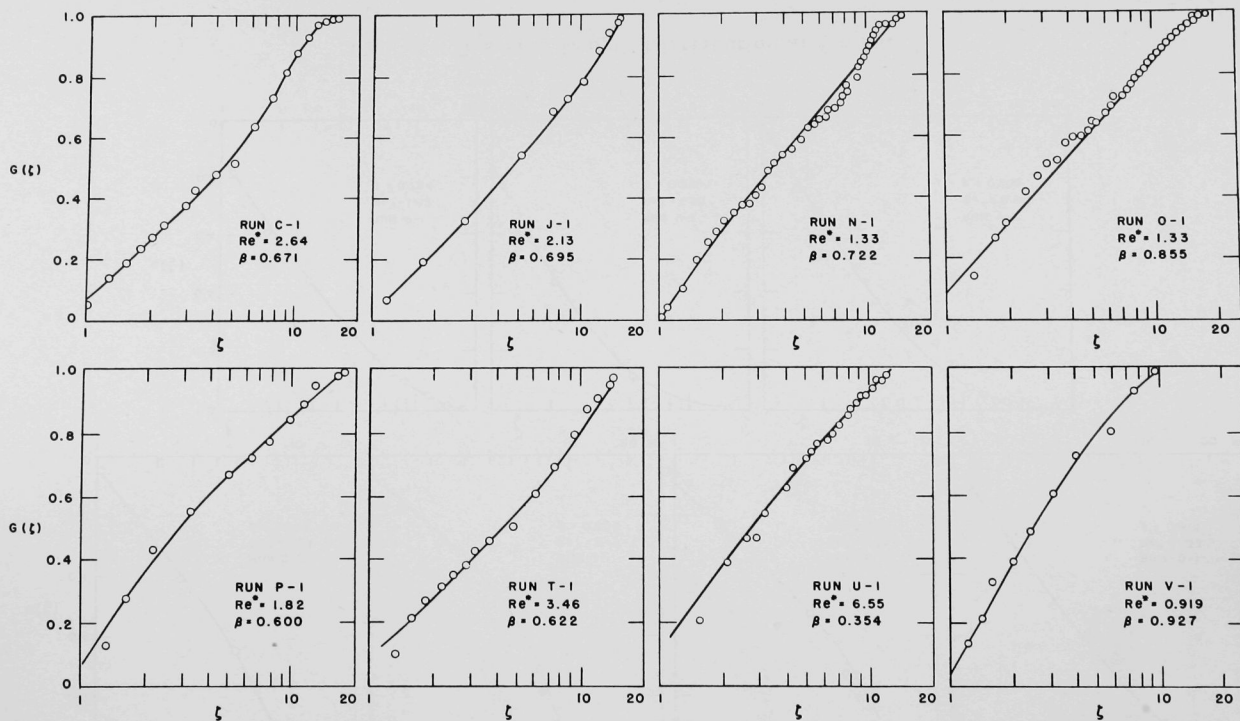


Fig. 22. Gas Slug Length Distribution at $\xi = 51.5$

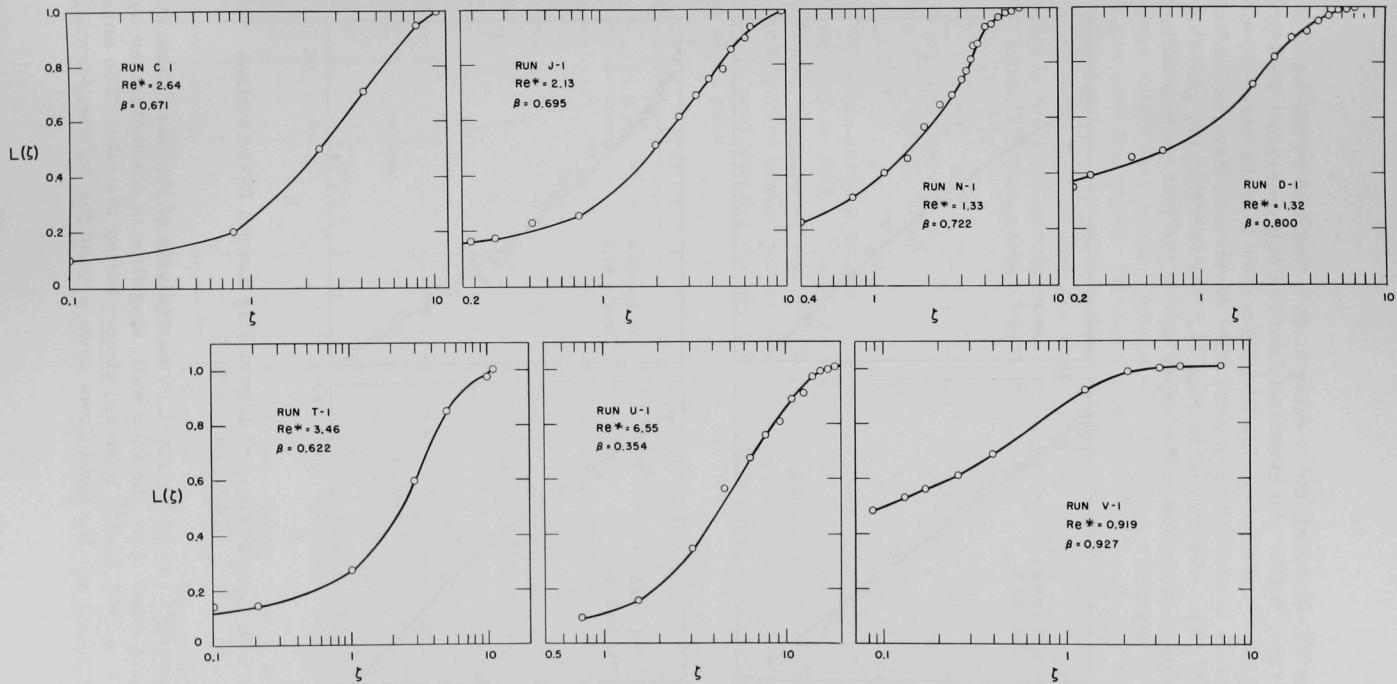


Fig. 23. Liquid Slug Length Distribution at $\xi = 51.5$

(about 6 in. in a 1-in. tube), the trailing slug, influenced by the wake of the leading one, rises faster and eventually the two agglomerate. This process is the last stage of developing slug flow. To show that the mercury-nitrogen flow of this study is stable and, hence, fully developed, distribution data at $\xi = 28.5$ and $\xi = 51.5$ are plotted in Fig. 24. The fact that the gas-slug-length distribution does not change in the upper half of the test section indicates that the flow is stable.

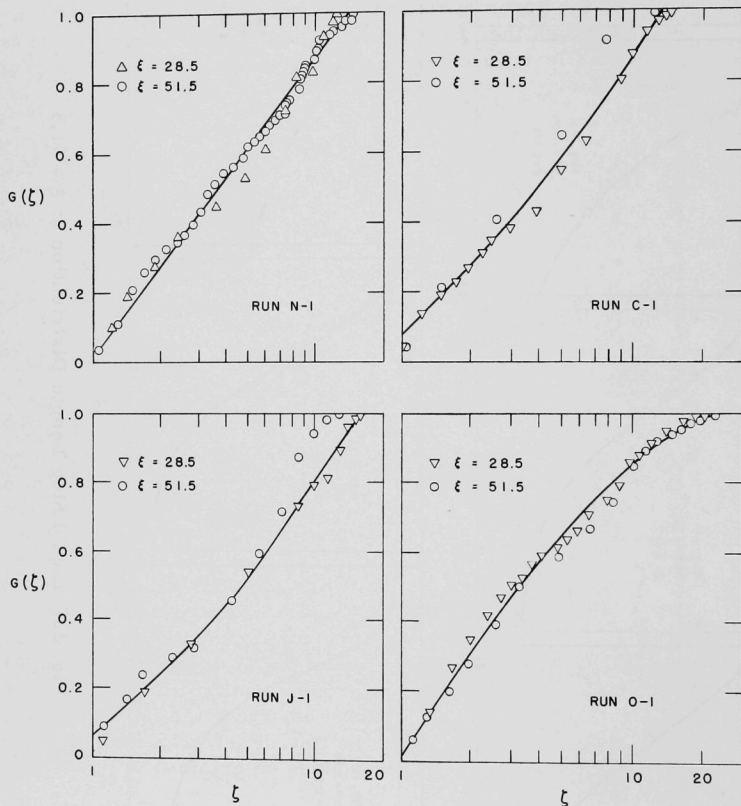


Fig. 24. Comparison of Liquid Slug Length Distributions at $\xi = 28.5$ and $\xi = 51.5$

The conflict can be resolved by an analysis of the basic flow structure. When the liquid wets the tube wall, slug flow is characterized by large bubbles, called Taylor bubbles, almost filling the tube. The nose of the bubble is round and the fluid flows down around the bubble, forming a

continuous film at the wall. The wake is a low-pressure region which attracts a trailing slug. When the liquid does not wet the tube wall, slug flow is characterized by alternating slugs of gas and liquid completely filling the tube cross section. The nose of the gas slug tends to be flat; however, shear at the wall distorts it to a slightly domed shape. For tube diameter smaller than some critical value, determined by Taylor instability,⁽⁴³⁾ the gas slugs retain this shape, completely filling the tube, and there is no slip of the gas past the liquid. However, when the tube diameter is greater than the critical value, the upper surface of the gas slug becomes unstable, and the liquid pours through the gas slug, resulting in slip. The critical tube diameter is the smallest diameter in which a surface wave can be propagated. Lamb⁽²⁶⁾ shows this to be

$$d_c = \pi \left[\frac{\sigma_1}{g(\rho_L - \rho_G)} \right]^{1/2}, \quad (5.19)$$

where σ_1 is the surface tension of the mercury-nitrogen interface, about 490 dynes/cm at 20°C. The value of d_c at this temperature is 0.23 in. In a 1-in. tube, there is no wake in the normal sense of a low-pressure region produced by flow around the bubble. Hence, a second slug may follow close behind. At equilibrium, the slugs may agglomerate, but they are produced at the same rate.

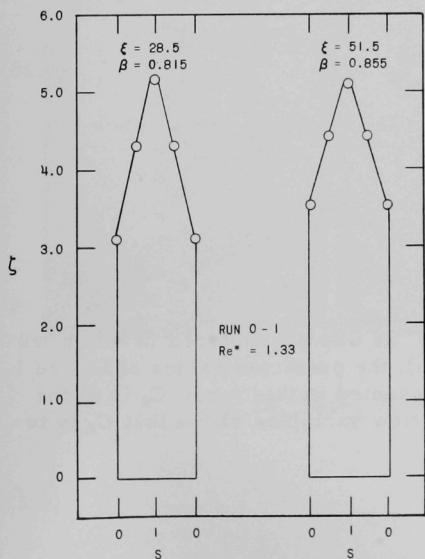


Fig. 25. Time Average Slug Shapes

Since mercury probably pours through the gas slug in an irregular fashion, the individual slugs will be asymmetrical at any instant. However, one would expect the time-averaged slug shape to be axisymmetrical. This average slug size and shape can be determined by measuring the average slug length from the photographic record of the probe signal at $S = 1, 0.5,$ and $0.06,$ and assuming the tail of the slug to be flat. Figure 25 shows typical slug shapes determined in this way.

These results prompted a visual study of the flow. A 3-ft length of glass pipe (of 1-in. diameter) was erected vertically. A rubber stopper with a nitrogen injector was inserted at the bottom and a mercury trap for entrained mercury was connected at the top.

Slugs of nitrogen were forced in the bottom and photographed as they rose through stagnant mercury. The largest slug which could be produced was 8 in. long.

The conclusion of an asymmetric slug (see above) was verified. The slugs, up to about 4 in. long, moved up one side wall, with the mercury falling down the opposite wall. As the slug rose, it slowly rotated inside the tube. Typical nitrogen-slug geometries are shown in Fig. 26. The shorter slugs (1 in. and 4 in. long) are shaped similarly to one-half of a Taylor slug. The bottoms are almost flat. The longer slugs (7 in. to 8 in. long) are spiral shaped. The probable explanation is that in rotating the bottom of the slug lags behind the top.

D. Slug Velocities

It was shown above that the liquid-velocity and the gas-fraction profiles are very flat, and the assumption of slug flow can be made. By means of the assumption of similar profiles for the liquid-velocity and gas-velocity profiles (which was made in modifying the variable-density model), the slug velocity, with respect to laboratory coordinates, is the same as the cross-sectional average gas velocity. Griffith and Wallis defined a slug velocity, with respect to the system, as the velocity of the gas slug with respect to the liquid well ahead of it. In the notation defined here, this is equivalent to the gas slip velocity. In their paper it was proposed to correlate the slug velocity as

$$U_s / 0.495 g D_p = C_2 \quad , \quad (5.20)$$

where C_2 is a parameter dependent upon the slug Reynolds number

$$Re_s = U_s D_p / U_L$$

and the stream Reynolds number

$$Re = V_{\text{Mix}} D_p / D_L \quad .$$

At very large values of these quantities, as was encountered in this work ($Re_s = 10,000$ and $Re = 9000$ minimum), the predicted values of C_2 are 1.0 or 1.1. However, when the data are presented in this form, C_2 is of the order 1.8. A correlation of C_2 with the flow variables shows that C_2 is independent of Re^* and is given by

$$C_2 = 1.05 / \beta^{0.76} \quad . \quad (5.21)$$

The error in this equation is $\pm 16\%$.

Considering the differences in the basic flow structure, it is not surprising that the theory for air-water slug flow does not predict the slug velocity in mercury-nitrogen flow.



8-IN. SLUG

4-IN. SLUG

1-IN. SLUG

Fig. 26. Nitrogen Slugs in Stagnant Mercury

VI. CONCLUSIONS

The gas-fraction and liquid-velocity profiles in fully developed flow can be expressed by power-law relationships. The exponents for these relationships have about the same magnitude and vary with the flow parameters in the same direction.

Entrance effects persist for about 20 tube diameters. In mercury-nitrogen flow, these are manifested by a large gas fraction at the wall, as well as large fluctuations of static pressure and a large phase-velocity ratio.

In mercury-nitrogen slug flow, the phase distribution is not important in determining the average phase-velocity ratio ($K = 1$), and all slip is due to local slip. Further, under the assumptions made in the modified variable-density model, the local slip is given by Eq. (5.9).

The empirical result of Armand:(1)

$$\bar{\alpha}/\beta = C \quad ,$$

is not valid for this study, since C is a function of the flow variables according to Eq. (5.12).

The gas slip velocity and the relative slip velocity are quantities which can be correlated reasonably accurately. For very large Reynolds numbers, as in this study ($Re > 9000$), these quantities are independent of Reynolds number, as shown in Eqs. (5.17) and (5.18). The liquid slip velocity, on the other hand, cannot be correlated accurately because it is such a small quantity.

The bubble diameter and slug (both gas and liquid) length spectra can be represented as a cumulative distribution function. These show that the large proportion of bubbles have $\zeta < 1$, but that most of the gas flow is carried by the slugs.

The basic flow structure of mercury-nitrogen flow is different from air-water flow as a result of the high surface energy of mercury; consequently, the theories derived from air-water flow cannot be used to predict flow variables.

The usual Taylor bubble does not appear. The gas slug rises up the wall, with the liquid pouring down the opposite wall. The slugs rotate as they rise, and very long gas slugs are spiral shaped.

The Griffith and Wallis slug-velocity correlation does not apply. A new correlation, using the same basis followed by Griffith and Wallis, was successfully made.

APPENDIX A
TABULATED DATA

Table A-1 (Contd.)

| T, °C | Re* | W _L , lb/sec | W _G (10 ⁴), lb/sec | Gas Fraction, α | | | | | | | | | | | | | | |
|----------------|------|----------------------------|--|-----------------|---------|-------|----------|--------|----------|--------|----------|--|--------------------------|------|------|-------|--|--|
| | | | | S | ξ = 5.7 | S | ξ = 17.1 | S | ξ = 28.5 | S | ξ = 51.5 | | P _r , psfa | β | | | | |
| <u>Run B-1</u> | | | | | | | | | | | | | | | | | | |
| 28 | 8.61 | 6.02 | 5.64 | 0.030 | 0.191 | | | 0.062 | 0.107 | 0.062 | 0.186 | | | | | | | |
| | | | | 0.149 | 0.144 | | | 0.181 | 0.136 | 0.122 | 0.224 | | | | | | | |
| | | | | 0.267 | 0.124 | | | 0.320 | 0.172 | 0.241 | 0.247 | | | | | | | |
| | | | | 0.366 | 0.144 | | | 0.439 | 0.182 | 0.360 | 0.284 | | | 5.7 | 6240 | 0.268 | | |
| | | | | 0.505 | 0.102 | | | 0.578 | 0.190 | 0.479 | 0.290 | | | 17.1 | 5410 | 0.303 | | |
| | | | | 0.605 | 0.093 | | | 0.697 | 0.209 | 0.598 | 0.304 | | | 28.5 | 4740 | 0.332 | | |
| | | | | 0.740 | 0.090 | | | 0.836 | 0.214 | 0.717 | 0.311 | | | 51.5 | 3420 | 0.407 | | |
| | | | | 0.840 | 0.092 | | | 0.906 | 0.211 | 0.836 | 0.320 | | | | | | | |
| | | | | 0.980 | 0.083 | | | 0.955 | 0.213 | 0.955 | 0.320 | | | | | | | |
| <u>Run R-1</u> | | | | | | | | | | | | | | | | | | |
| 27 | 7.84 | 5.46 | 4.29 | 0.030 | 0.025 | 0.047 | 0.053 | 0.062 | 0.079 | 0.062 | 0.150 | | | | | | | |
| | | | | 0.149 | 0.014 | 0.078 | 0.077 | 0.181 | 0.094 | 0.122 | 0.203 | | | | | | | |
| | | | | 0.267 | 0.011 | 0.203 | 0.081 | 0.320 | 0.104 | 0.241 | 0.225 | | | | | | | |
| | | | | 0.505 | 0.0125 | 0.328 | 0.081 | 0.578 | 0.122 | 0.479 | 0.256 | | | 5.7 | 5850 | 0.252 | | |
| | | | | 0.740 | 0.011 | 0.578 | 0.086 | 0.836 | 0.128 | 0.717 | 0.267 | | | 17.1 | 5100 | 0.278 | | |
| | | | | 0.980 | 0.0098 | 0.828 | 0.088 | 0.906 | 0.131 | 0.955 | 0.267 | | | 28.5 | 4370 | 0.310 | | |
| | | | | | | 0.922 | 0.093 | | | | | | | 51.5 | 3010 | 0.395 | | |
| <u>Run U-1</u> | | | | | | | | | | | | | | | | | | |
| 29 | 6.55 | 4.52 | 2.88 | 0.030 | 0.011 | 0.047 | 0.047 | 0.062 | 0.0875 | 0.062 | 0.115 | | | | | | | |
| | | | | 0.149 | 0.011 | 0.078 | 0.056 | 0.181 | 0.075 | 0.122 | 0.152 | | | | | | | |
| | | | | 0.267 | 0.0125 | 0.203 | 0.059 | 0.320 | 0.076 | 0.241 | 0.16 | | | 5.7 | 5290 | 0.232 | | |
| | | | | 0.505 | 0.014 | 0.328 | 0.056 | 0.578 | 0.093 | 0.479 | 0.187 | | | 17.1 | 4520 | 0.262 | | |
| | | | | 0.740 | 0.014 | 0.578 | 0.056 | 0.836 | 0.90 | 0.717 | 0.19 | | | 28.5 | 3760 | 0.299 | | |
| | | | | 0.980 | 0.014 | 0.828 | 0.056 | 0.906 | 0.089 | 0.955 | 0.19 | | | 51.5 | 2300 | 0.354 | | |
| | | | | | | 0.922 | 0.056 | | | | | | | | | | | |
| <u>Run A-2</u> | | | | | | | | | | | | | | | | | | |
| 26 | 14.5 | 10.15 | 8.25 | 0.0595 | 0.112 | | | 0.595 | 0.0919 | 0.038 | 0.095 | | | | | | | |
| | | | | 0.208 | 0.0874 | | | 0.268 | 0.161 | 0.237 | 0.240 | | | 5.7 | 5710 | 0.262 | | |
| | | | | 0.446 | 0.0860 | | | 0.506 | 0.184 | 0.356 | 0.276 | | | 17.1 | 4990 | | | |
| | | | | 0.683 | 0.0794 | | | 0.745 | 0.203 | 0.596 | 0.310 | | | 28.5 | 4300 | 0.319 | | |
| | | | | 0.925 | 0.0815 | | | 0.985 | 0.206 | 0.833 | 0.323 | | | 51.5 | 2970 | 0.397 | | |
| | | | | | | | | | | 0.930 | 0.329 | | | | | | | |
| <u>Run B-2</u> | | | | | | | | | | | | | | | | | | |
| 27 | 13.2 | 9.29 | 5.77 | 0.0595 | 0.104 | | | 0.0595 | 0.0705 | 0.038 | 0.069 | | | | | | | |
| | | | | 0.208 | 0.0704 | | | 0.268 | 0.1169 | 0.356 | 0.211 | | | 5.7 | 5850 | 0.211 | | |
| | | | | 0.446 | 0.0521 | | | 0.506 | 0.138 | 0.596 | 0.220 | | | 17.1 | 5110 | | | |
| | | | | 0.683 | 0.0431 | | | 0.745 | 0.151 | 0.833 | 0.228 | | | 28.5 | 4410 | 0.262 | | |
| | | | | 0.925 | 0.0374 | | | 0.985 | 0.152 | 0.930 | 0.255 | | | 51.5 | 3000 | 0.344 | | |
| <u>Run C-2</u> | | | | | | | | | | | | | | | | | | |
| 27 | 11.7 | 8.16 | 4.11 | 0.0595 | 0.0952 | | | 0.0595 | 0.0374 | 0.0595 | 0.091 | | | | | | | |
| | | | | 0.208 | 0.0500 | | | 0.268 | 0.0816 | 0.356 | 0.150 | | | 5.7 | 6000 | 0.174 | | |
| | | | | 0.446 | 0.0340 | | | 0.506 | 0.103 | 0.596 | 0.159 | | | 17.1 | 5510 | | | |
| | | | | 0.683 | 0.0295 | | | 0.745 | 0.114 | 0.833 | 0.162 | | | 28.5 | 4470 | 0.220 | | |
| | | | | 0.925 | 0.0238 | | | 0.985 | 0.110 | 0.930 | 0.163 | | | 51.5 | 3040 | 0.292 | | |
| <u>Run D-2</u> | | | | | | | | | | | | | | | | | | |
| 28 | 10.0 | 7.05 | 2.71 | 0.060 | 0.0715 | | | 0.0595 | 0.042 | 0.0595 | 0.0635 | | | | | | | |
| | | | | 0.208 | 0.0317 | | | 0.268 | 0.055 | 0.356 | 0.104 | | | 5.7 | 6000 | 0.174 | | |
| | | | | 0.446 | 0.0159 | | | 0.506 | 0.059 | 0.596 | 0.116 | | | 17.1 | 5380 | | | |
| | | | | 0.683 | 0.0136 | | | 0.745 | 0.060 | 0.833 | 0.124 | | | 28.5 | 4620 | 0.167 | | |
| | | | | 0.925 | 0.0125 | | | 0.985 | 0.059 | 0.930 | 0.127 | | | 51.5 | 3100 | 0.230 | | |
| <u>Run F-2</u> | | | | | | | | | | | | | | | | | | |
| 28 | 13.8 | 9.67 | 6.98 | 0.0595 | 0.094 | | | 0.595 | 0.050 | 0.0595 | 0.127 | | | | | | | |
| | | | | 0.208 | 0.0645 | | | 0.268 | 0.127 | 0.356 | 0.220 | | | 5.7 | 5800 | 0.240 | | |
| | | | | 0.446 | 0.565 | | | 0.506 | 0.157 | 0.596 | 0.235 | | | 17.1 | 5060 | | | |
| | | | | 0.683 | 0.0510 | | | 0.745 | 0.163 | 0.833 | 0.254 | | | 28.5 | 4350 | 0.296 | | |
| | | | | 0.925 | 0.0397 | | | 0.985 | 0.172 | 0.930 | 0.270 | | | 51.5 | 2990 | 0.380 | | |

Table A-1 (Contd.)

| T, °C | Re* | W _L , lb/sec | W _G (10 ⁴), lb/sec | Gas Fraction, | | | | | | | P, psfa | β | | | | | |
|----------|-------|----------------------------|--|---------------|---------|--------|----------|-------|----------|-------|------------|---|------------|---|------|------|-------|
| | | | | S | ξ = 5.7 | S | ξ = 17.1 | S | ξ = 28.5 | S | | | ξ = 51.5 | | | | |
| Run D-1 | | | | | | | | | | | | | | | | | |
| 31 | 2.04 | 1.40 | 2.01 | 0.030 | 0.072 | | | 0.062 | 0.106 | 0.062 | 0.159 | ξ | P, psfa | β | | | |
| | | | | 0.149 | 0.065 | | | 0.181 | 0.113 | 0.187 | 0.175 | | | | | | |
| | | | | 0.267 | 0.061 | | | 0.320 | 0.114 | 0.312 | 0.184 | | | | | | |
| | | | | 0.366 | 0.057 | | | 0.439 | 0.122 | 0.437 | 0.185 | | | | 5.7 | 5840 | 0.386 |
| | | | | 0.505 | 0.053 | | | 0.578 | 0.124 | 0.562 | 0.186 | | | | 17.1 | 5055 | 0.417 |
| | | | | 0.605 | 0.049 | | | 0.697 | 0.118 | 0.687 | 0.206 | | | | 28.5 | 4310 | 0.457 |
| | | | | 0.743 | 0.045 | | | 0.836 | 0.124 | 0.812 | 0.205 | | | | 51.5 | 2865 | 0.559 |
| | | | | 0.842 | 0.045 | | | 0.906 | 0.123 | 0.938 | | | | | | | |
| | | | | 0.980 | 0.044 | | | 0.955 | 0.123 | | | | | | | | |
| | | | | | | | | | | | | | | | | | |
| Run F-1 | | | | | | | | | | | | | | | | | |
| 24 | 0.796 | 0.563 | 6.49 | 0.030 | 0.088 | 0.0468 | 0.209 | 0.062 | 0.351 | 0.187 | 0.256 | ξ | P, psfa | β | | | |
| | | | | 0.149 | 0.057 | 0.172 | 0.227 | 0.181 | 0.386 | 0.312 | 0.334 | | | | | | |
| | | | | 0.267 | 0.059 | 0.297 | 0.242 | 0.320 | 0.416 | 0.437 | 0.433 | | | | | | |
| | | | | 0.366 | 0.065 | 0.422 | 0.281 | 0.439 | 0.416 | 0.562 | 0.439 | | | | 5.7 | 4640 | 0.860 |
| | | | | 0.505 | 0.083 | 0.547 | 0.263 | 0.578 | 0.425 | 0.687 | 0.458 | | | | 17.1 | 4040 | 0.872 |
| | | | | 0.605 | 0.093 | 0.672 | 0.306 | 0.697 | 0.443 | 0.812 | 0.446 | | | | 28.5 | 3510 | 0.890 |
| | | | | 0.743 | 0.103 | 0.797 | 0.338 | 0.836 | 0.450 | 0.937 | 0.442 | | | | 51.5 | 2510 | 0.920 |
| | | | | 0.842 | 0.117 | 0.922 | 0.349 | 0.906 | 0.451 | 0.938 | 0.456 | | | | | | |
| | | | | 0.980 | 0.125 | 0.953 | 0.345 | 0.955 | 0.464 | | | | | | | | |
| | | | | | | | | | | | | | | | | | |
| Run H-1 | | | | | | | | | | | | | | | | | |
| 24 | 2.20 | 1.55 | 2.89 | 0.030 | 0.025 | 0.047 | 0.096 | 0.062 | 0.131 | 0.062 | 0.207 | ξ | P, psfa | β | | | |
| | | | | 0.149 | 0.010 | 0.110 | 0.098 | 0.181 | 0.149 | 0.187 | 0.237 | | | | | | |
| | | | | 0.267 | 0.010 | 0.235 | 0.102 | 0.320 | 0.176 | 0.312 | 0.259 | | | | | | |
| | | | | 0.366 | 0.011 | 0.360 | 0.123 | 0.439 | 0.182 | 0.437 | 0.258 | | | | 5.7 | 5640 | 0.450 |
| | | | | 0.505 | 0.018 | 0.485 | 0.134 | 0.578 | 0.184 | 0.562 | 0.270 | | | | 17.1 | 4890 | 0.486 |
| | | | | 0.605 | 0.018 | 0.610 | 0.138 | 0.697 | 0.188 | 0.687 | 0.278 | | | | 28.5 | 4160 | 0.526 |
| | | | | 0.743 | 0.018 | 0.735 | 0.138 | 0.836 | 0.182 | 0.812 | 0.275 | | | | 51.5 | 2860 | 0.616 |
| | | | | 0.842 | 0.020 | 0.860 | 0.138 | 0.906 | 0.182 | 0.937 | 0.298 | | | | | | |
| | | | | 0.980 | 0.021 | 0.985 | 0.142 | 0.955 | 0.185 | 0.938 | 0.280 | | | | | | |
| | | | | | | | | | | | | | | | | | |
| Run I-1 | | | | | | | | | | | | | | | | | |
| 24 | 2.82 | 2.00 | 4.52 | 0.030 | 0.072 | | | 0.062 | 0.270 | 0.062 | 0.332 | ξ | P, psfa | β | | | |
| | | | | 0.149 | 0.0416 | | | 0.181 | 0.317 | 0.187 | 0.397 | | | | | | |
| | | | | 0.267 | 0.0541 | | | 0.320 | 0.346 | 0.312 | 0.422 | | | | | | |
| | | | | 0.366 | 0.0653 | | | 0.439 | 0.361 | 0.437 | 0.430 | | | | 5.7 | 5100 | 0.525 |
| | | | | 0.505 | 0.0764 | | | 0.578 | 0.380 | 0.562 | 0.439 | | | | 17.1 | 4460 | 0.556 |
| | | | | 0.605 | 0.0834 | | | 0.697 | 0.388 | 0.687 | 0.459 | | | | 28.5 | 3880 | 0.590 |
| | | | | 0.743 | 0.104 | | | 0.836 | 0.385 | 0.812 | 0.467 | | | | 51.5 | 2820 | 0.665 |
| | | | | 0.840 | 0.104 | | | 0.906 | 0.392 | 0.937 | 0.465 | | | | | | |
| | | | | 0.980 | 0.104 | | | 0.955 | 0.398 | 0.938 | 0.472 | | | | | | |
| | | | | | | | | | | | | | | | | | |
| Run K-1 | | | | | | | | | | | | | | | | | |
| 25 | 1.84 | 1.295 | 3.81 | 0.030 | 0.0166 | 0.047 | 0.114 | 0.062 | 0.152 | 0.062 | 0.250 | ξ | P, psfa | β | | | |
| | | | | 0.149 | 0.0139 | 0.078 | 0.125 | 0.181 | 0.219 | 0.187 | 0.320 | | | | | | |
| | | | | 0.267 | 0.0180 | 0.203 | 0.170 | 0.320 | 0.234 | 0.312 | 0.338 | | | | 5.7 | 5530 | 0.565 |
| | | | | 0.505 | 0.0278 | 0.328 | 0.179 | 0.578 | 0.259 | 0.562 | 0.377 | | | | 17.1 | 4810 | 0.599 |
| | | | | 0.743 | 0.0347 | 0.578 | 0.185 | 0.697 | 0.252 | 0.687 | 0.360 | | | | 28.5 | 4140 | 0.633 |
| | | | | 0.980 | 0.0431 | 0.828 | 0.201 | 0.836 | 0.248 | 0.812 | 0.364 | | | | 51.5 | 3040 | 0.701 |
| | | | | | | 0.922 | 0.192 | 0.906 | 0.261 | 0.937 | 0.360 | | | | | | |
| | | | | | | | | 0.955 | 0.275 | 0.938 | 0.373 | | | | | | |
| | | | | | | | | | | | | | | | | | |
| | | | | | | | | | | | | | | | | | |
| Run L-1 | | | | | | | | | | | | | | | | | |
| 26 | 1.25 | 0.874 | 3.81 | 0.030 | 0.025 | 0.047 | 0.126 | 0.062 | 0.183 | 0.062 | 0.297 | ξ | P, psfa | β | | | |
| | | | | 0.149 | 0.0167 | 0.078 | 0.150 | 0.181 | 0.224 | 0.187 | 0.320 | | | | | | |
| | | | | 0.267 | 0.0264 | 0.203 | 0.183 | 0.320 | 0.250 | 0.312 | 0.365 | | | | | | |
| | | | | 0.505 | 0.0333 | 0.328 | 0.181 | 0.439 | 0.265 | 0.562 | 0.379 | | | | 5.7 | 5150 | 0.681 |
| | | | | 0.743 | 0.0362 | 0.453 | 0.187 | 0.578 | 0.285 | 0.812 | 0.371 | | | | 17.1 | 4450 | 0.710 |
| | | | | 0.980 | 0.0473 | 0.578 | 0.1765 | 0.836 | 0.289 | 0.938 | 0.389 | | | | 28.5 | 3850 | 0.740 |
| | | | | | | 0.703 | 0.208 | 0.906 | 0.293 | | | | | | 51.5 | 2780 | 0.796 |
| | | | | | | 0.828 | 0.195 | | | | | | | | | | |
| | | | | | | 0.922 | 0.216 | | | | | | | | | | |
| | | | | | | 0.953 | 0.224 | | | | | | | | | | |

Table A-4

ARMAND'S PARAMETER

| Run No. | ξ | $\bar{\alpha}$ | β | C | δ | Run No. | ξ | $\bar{\alpha}$ | β | C | δ |
|-----------------|-------|----------------|---------|-------|----------|---------|-------|----------------|---------|-------|----------|
| C-1 | 28.5 | 0.282 | 0.589 | 0.479 | 0.007 | D-2 | 28.5 | 0.056 | 0.168 | 0.333 | 0.139 |
| | 51.5 | 0.365 | 0.671 | 0.543 | 0.071 | | 51.5 | 0.108 | 0.230 | 0.470 | 0.002 |
| J-1 | 28.5 | 0.222 | 0.609 | 0.365 | 0.107 | F-2 | 28.5 | 0.139 | 0.396 | 0.470 | 0.002 |
| | 51.5 | 0.337 | 0.695 | 0.485 | 0.013 | | 51.5 | 0.213 | 0.380 | 0.560 | 0.088 |
| N-1 | 28.5 | 0.205 | 0.652 | 0.315 | 0.157 | D-1 | 28.5 | 0.116 | 0.457 | 0.254 | 0.218 |
| | 51.5 | 0.316 | 0.722 | 0.438 | 0.034 | | 51.5 | 0.194 | 0.557 | 0.348 | 0.124 |
| O-1 | 28.5 | 0.355 | 0.815 | 0.435 | 0.037 | F-1 | 28.5 | 0.400 | 0.890 | 0.450 | 0.222 |
| | 51.5 | 0.457 | 0.855 | 0.535 | 0.063 | | 51.5 | 0.428 | 0.920 | 0.465 | 0.007 |
| P-1 | 28.5 | 0.321 | 0.748 | 0.430 | 0.042 | H-1 | 28.5 | 0.165 | 0.526 | 0.313 | 0.159 |
| | 51.5 | 0.432 | 0.800 | 0.540 | 0.068 | | 51.5 | 0.255 | 0.616 | 0.413 | 0.059 |
| T-1 | 28.5 | 0.221 | 0.535 | 0.413 | 0.059 | I-1 | 28.5 | 0.343 | 0.590 | 0.581 | 0.109 |
| | 51.5 | 0.358 | 0.622 | 0.575 | 0.103 | | 51.5 | 0.428 | 0.665 | 0.643 | 0.171 |
| V-1 | 28.5 | 0.460 | 0.905 | 0.509 | 0.037 | K-1 | 28.5 | 0.249 | 0.633 | 0.394 | 0.078 |
| | 51.5 | 0.579 | 0.927 | 0.625 | 0.153 | | 51.5 | 0.337 | 0.701 | 0.480 | 0.008 |
| B-1 | 28.5 | 0.169 | 0.332 | 0.510 | 0.038 | L-1 | 28.5 | 0.260 | 0.740 | 0.352 | 0.120 |
| | 51.5 | 0.277 | 0.407 | 0.680 | 0.208 | | 51.5 | 0.358 | 0.796 | 0.450 | 0.022 |
| R-1 | 28.5 | 0.111 | 0.310 | 0.358 | 0.114 | M-1 | 28.5 | 0.164 | 0.587 | 0.280 | 0.192 |
| | 51.5 | 0.234 | 0.395 | 0.592 | 0.120 | | 51.5 | 0.269 | 0.679 | 0.396 | 0.076 |
| U-1 | 28.5 | 0.087 | 0.299 | 0.291 | 0.181 | Q-1 | 28.5 | 0.290 | 0.661 | 0.439 | 0.033 |
| | 51.5 | 0.171 | 0.354 | 0.484 | 0.012 | | 51.5 | 0.395 | 0.727 | 0.343 | 0.071 |
| A-2 | 28.5 | 0.172 | 0.319 | 0.540 | 0.068 | S-1 | 28.5 | 0.188 | 0.442 | 0.425 | 0.047 |
| | 51.5 | 0.273 | 0.397 | 0.687 | 0.215 | | 51.5 | 0.309 | 0.535 | 0.578 | 0.106 |
| B-2 | 28.5 | 0.128 | 0.262 | 0.489 | 0.017 | W-1 | 28.5 | 0.415 | 0.869 | 0.478 | 0.006 |
| | 51.5 | 0.215 | 0.344 | 0.625 | 0.153 | | 51.5 | 0.509 | 0.878 | 0.579 | 0.107 |
| C-2 | 28.5 | 0.094 | 0.220 | 0.427 | 0.045 | | | | | | |
| | 51.5 | 0.146 | 0.292 | 0.500 | 0.028 | | | | | | |
| Average Values: | | | | | | | | | | 0.472 | 0.083 |

Table A-5
AVERAGE AND SLIP VELOCITY DATA

| Run No. | ξ | V_{Mix} | \bar{U}_G | \bar{U}_L | u_G | $-u_L$ | u_R |
|---------|-------|-----------|-------------|-------------|-------|--------|-------|
| C-1 | 28.5 | 0.87 | 1.83 | 0.50 | 0.96 | 0.37 | 1.33 |
| | 51.5 | 1.00 | 1.77 | 0.56 | 0.77 | 0.44 | 1.21 |
| J-1 | 28.5 | 0.74 | 2.00 | 0.380 | 1.26 | 0.36 | 1.62 |
| | 51.5 | 0.963 | 1.99 | 0.445 | 1.03 | 0.52 | 1.54 |
| N-1 | 28.5 | 0.527 | 1.67 | 0.23 | 1.14 | 0.30 | 1.44 |
| | 51.5 | 0.665 | 1.52 | 0.27 | 0.86 | 0.39 | 1.25 |
| O-1 | 28.5 | 1.00 | 2.30 | 0.287 | 1.30 | 0.71 | 2.01 |
| | 51.5 | 1.28 | 2.39 | 0.341 | 1.11 | 0.44 | 2.05 |
| P-1 | 28.5 | 1.00 | 2.30 | 0.371 | 1.30 | 0.63 | 1.93 |
| | 51.5 | 1.25 | 2.31 | 0.444 | 1.06 | 0.81 | 1.87 |
| T-1 | 28.5 | 1.01 | 2.45 | 0.609 | 1.44 | 0.40 | 1.84 |
| | 51.5 | 1.25 | 2.17 | 0.737 | 0.92 | 0.51 | 1.43 |
| V-1 | 28.5 | 1.31 | 2.58 | 0.232 | 1.27 | 1.08 | 2.35 |
| | 51.5 | 1.74 | 2.78 | 0.298 | 1.04 | 1.44 | 2.48 |
| B-1 | 28.5 | 1.78 | 3.48 | 1.43 | 1.70 | 0.35 | 2.05 |
| | 51.5 | 2.00 | 2.95 | 1.62 | 0.95 | 0.36 | 1.31 |
| R-1 | 28.5 | 1.56 | 3.73 | 1.21 | 2.17 | 0.35 | 2.52 |
| | 51.5 | 1.78 | 3.0 | 1.41 | 1.22 | 0.39 | 2.59 |
| U-1 | 28.5 | 1.28 | 3.64 | 1.00 | 2.36 | 0.28 | 2.64 |
| | 51.5 | 1.51 | 3.64 | 1.10 | 2.13 | 0.41 | 1.54 |
| A-2 | 28.5 | 2.98 | 5.53 | 2.42 | 2.55 | 0.56 | 3.11 |
| | 51.5 | 3.35 | 4.89 | 2.72 | 1.54 | 0.83 | 2.17 |
| B-2 | 28.5 | 2.48 | 5.08 | 2.10 | 2.60 | 0.38 | 2.98 |
| | 51.5 | 2.80 | 4.48 | 2.33 | 1.68 | 0.47 | 2.15 |
| C-2 | 28.5 | 2.07 | 4.85 | 1.78 | 2.78 | 0.29 | 3.07 |
| | 51.5 | 2.28 | 4.55 | 1.89 | 2.28 | 0.39 | 2.66 |
| D-2 | 28.5 | 1.74 | 5.20 | 1.48 | 3.46 | 0.26 | 3.73 |
| | 51.5 | 1.89 | 4.03 | 1.56 | 2.14 | 0.33 | 2.47 |
| F-2 | 28.5 | 2.71 | 5.75 | 2.22 | 3.04 | 0.49 | 3.53 |
| | 51.5 | 3.07 | 5.48 | 2.43 | 2.41 | 0.64 | 3.05 |
| D-1 | 28.5 | 0.508 | 1.99 | 0.312 | 1.48 | 0.196 | 1.68 |
| | 51.5 | 0.625 | 1.79 | 0.340 | 1.17 | 0.285 | 1.45 |
| F-1 | 28.5 | 1.01 | 2.23 | 0.184 | 1.22 | 0.83 | 2.05 |
| | 51.5 | 1.39 | 2.91 | 0.192 | 1.52 | 1.20 | 2.72 |
| H-1 | 28.5 | 0.645 | 2.05 | 0.365 | 1.41 | 0.28 | 1.68 |
| | 51.5 | 0.796 | 1.93 | 0.410 | 1.13 | 0.39 | 1.52 |
| I-1 | 28.5 | 0.96 | 1.65 | 0.60 | 0.69 | 0.36 | 1.05 |
| | 51.5 | 1.18 | 1.82 | 0.69 | 0.64 | 0.49 | 1.131 |
| K-1 | 28.5 | 0.705 | 1.80 | 0.339 | 1.09 | 0.366 | 1.46 |
| | 51.5 | 0.867 | 1.81 | 0.385 | 0.94 | 0.482 | 1.42 |
| L-1 | 28.5 | 0.659 | 1.87 | 0.233 | 1.21 | 0.426 | 1.64 |
| | 51.5 | 0.845 | 1.88 | 0.269 | 1.04 | 0.576 | 1.61 |
| M-1 | 28.5 | 0.596 | 2.13 | 0.295 | 1.53 | 0.301 | 1.84 |
| | 51.5 | 0.770 | 1.94 | 0.338 | 1.17 | 0.432 | 1.60 |
| Q-1 | 28.5 | 1.14 | 2.60 | 0.545 | 1.46 | 0.60 | 2.06 |
| | 51.5 | 1.41 | 2.60 | 0.639 | 1.19 | 0.77 | 1.96 |
| S-1 | 28.5 | 1.15 | 2.71 | 0.791 | 1.56 | 0.36 | 1.92 |
| | 51.5 | 1.38 | 2.40 | 0.93 | 1.02 | 0.45 | 1.47 |
| W-1 | 28.5 | 1.16 | 2.37 | 0.255 | 1.21 | 0.90 | 2.12 |
| | 51.5 | 1.45 | 2.56 | 0.303 | 1.11 | 1.15 | 2.26 |

BIBLIOGRAPHY

1. A. A. Armand, Frictional Forces for Two-phase Flow in Horizontal Tubes, Izvestia VTI, n1, 16-22 (1946).
2. A. A. Armand and G. G. Treschev, Investigation of Frictional Resistance for Flow of Water-Steam Mixtures in a Heated Boiler Tube at High Pressures, Izvestia VTI, n4, 1-5 (1947).
3. S. G. Bankoff, A Variable Density Single Fluid Model for Two-phase Flow with Particular Reference to Steam-Water Flow, J. Heat Transfer, Trans. Am. Soc. Mech. Engrs., Series C, 82, 265 (1960).
4. E. A. Budge, A New Form of Bubble Counter for Measurement of Gas Evolution, J. Am. Chem. Soc., 53, 2451 (1931).
5. S. Calvert and B. Williams, Upward Co-current Annular Flow of Air and Water in Smooth Tubes, A.I.Ch.E.J., 1, 78 (1955).
6. W. H. Cook, Boiling Density in Vertical Rectangular Multi-channel Sections with Natural Circulation, ANL-5621 (1956).
7. W. F. Davidson et al., Studies of Heat Transmission through Boiler Tubing at Pressures from 500 to 3300 Pounds, Trans. Am. Soc. Mech. Engrs., 65, 553 (1943).
8. R. M. Davies and G. I. Taylor, The Mechanics of Large Bubbles Rising through Extended Liquids and through Liquids in Tubes, Proc. Roy. Soc. (London), 200(A), 375 (1950).
9. C. E. Dengler, Heat Transfer and Pressure Drop for Evaporation of Water in a Vertical Tube, Ph.D. Thesis, M.I.T. (1952).
10. A. E. Dukler, Fluid Mechanics and Heat Transfer in Falling Film Systems, A.S.M.E.-A.I.Ch.E., Third National Heat Transfer Conference (August, 1959).
11. D. T. Dumetrescu, Motion of an Air Bubble in a Vertical Tube, Zamm, 23, n2, 139 (1943).
12. R. A. Egen, D. E. Dingee, and J. W. Chastain, Vapor Formation and Behavior in Boiling Heat Transfer, BMI-1163 (1957).
13. W. G. Eversole, G. H. Wagner, and E. Stackhaus, Rapid Formation of Gas Bubbles in Liquids, Ind. Eng. Chem., 33, 1459 (1941).

14. H. P. Grace and C. E. Lapple, Discharge Coefficients of Small Diameter Orifices and Flow Nozzles, Trans. Am. Soc. Mech. Engrs., 73, 639 (1951).
15. P. Griffith, J. A. Clark, and W. M. Rohsenow, Void Volumes in Subcooled Boiling Systems, A.S.M.E. Paper 58-HT-19 (1958).
16. P. Griffith and G. B. Wallis, Slug Flow, Technical Report 15, Division of Sponsored Research, M.I.T., NP-7779 (1959).
17. G. F. Hewitt, Analysis of Annular Two-phase Flow: Application of the Dukler Analysis to Vertical Upward Flow in a Tube, AERE R-3680 (1961).
18. J. O. Hinze, Turbulence, McGraw-Hill Book Company, Inc., New York (1959).
19. H. H. Hooker and G. F. Popper, A Gamma-ray Attenuation Method for Void Fraction Determinations in Experimental Boiling Heat Transfer Test Facilities, ANL-5766 (1958).
20. G. A. Hughmark, Holdup in Gas-Liquid Flow, Chem. Eng. Prog., 58, 62 (1962).
21. H. S. Isbin, R. H. Moen, and D. R. Mosher, Two-phase Pressure Drops, AECU-2994 (1954).
22. H. A. Johnson and A. H. Abou-Sabe, Heat Transfer and Pressure Drop for Turbulent Flow of Air-Water Mixtures in a Horizontal Pipe, Trans. Am. Soc. Mech. Engrs., 74 977 (1952).
23. S. I. Kosterin, Investigation of Hydraulic Friction from Two-phase Flow in Horizontal Tubes, Izvestia-Akademiia Nauk, SSSR-Otdelenie Tekhnicheskikh Nauk, 1864 (1949).
24. L. I. Krasiakova, Some Characteristics of Flow of a Two-phase Mixture in a Horizontal Pipe, Zhurnal Technicheskoi Fiziki, 22, n4, 656 (1952).
25. A. D. K. Laird and D. Chisholm, Pressure and Forces along Cylindrical Bubbles in a Vertical Tube, Ind. Eng. Chem., 48, 1361 (1956).
26. H. Lamb, Hydrodynamics, Dover Publications, New York (1932).
27. P. M. C. Lacey, G. F. Hewitt, and J. G. Collier, Climbing Film Flow, AERE-3962 (1962).

28. S. Levy, Steam Slip-Theoretical Prediction from Momentum Model, J. Heat Transfer, Trans. Am. Soc. Mech. Engrs., Series C, 82, 113 (1960).
29. S. Levy, Theory of Pressure Drop and Heat Transfer for Annular Steady State Two-phase, Two-component Flow in Pipes, The Second Midwestern Conference on Fluid Mechanics, (1952), p. 337.
30. R. W. Lockhart and R. C. Martinelli, Proposed Correlation of Data for Isothermal Two-phase, Two-component Flow in Pipes, Chem. Eng. Prog., 45, 39 (1949).
31. P. A. Lottes, M. Petrick, and J. F. Marchaterre, Lecture Notes on Heat Extraction from Boiling Water Power Reactors, ANL-6063 (1959).
32. Maung Maung-Myint, A Literature Survey on Two-phase Flow of Gas and Liquid, B.S. Thesis, M.I.T. (1959).
33. R. C. Martinelli et al., Isothermal Pressure Drop for Two-phase Two-component Flow in a Horizontal Pipe, Trans. Am. Soc. Mech. Engrs., 66, 139 (1944).
34. R. C. Martinelli and D. B. Nelson, Prediction of Pressure Drop during Forced Circulation Boiling of Water, Trans. Am. Soc. Mech. Engrs., 70, 695 (1948).
35. H. N. McManus, An Experimental Investigation of Film Characteristics in Horizontal Annular Two-phase Flow, A.S.M.E. Paper 57-A-144 (1958).
36. R. Moissis and P. Griffith, Entrance Effects in Two-phase Slug Flow, J. Heat Transfer, Trans. Am. Soc. Mech. Engrs., Series C, 84, 29 (1962).
37. A. O. Newman and B. J. Lerner, Electronic Method for Bubble Frequency Measurements, Anal. Chem., 26, 417 (1954).
38. H. C. Perkins, Jr., M. Yusuf, and G. Leppert, A Void Measurement Technique for Local Boiling, Nuclear Sci. Eng., 1, 525 (1960).
39. M. Petrick, Two-phase Air-Water Flow Phenomena, ANL-5787 (1958).
40. B. L. Richardson, Some Problems in Horizontal Two-phase Two-component Flow, ANL-5949 (1959).

41. H. Schlichting, Boundary Layer Theory, Pergamon Press, New York (1955).
42. Kinetic Studies of Heterogeneous Water Reactors, STL Report 8977-0011-SU-000, Quarterly Report for Period Ending September 30, 1961.
43. G. I. Taylor, The Instability of Liquid Surfaces when Accelerated in a Direction Perpendicular to Their Planes, Proc. Roy. Soc. (London), A201, 192 (1950).
44. J. H. Vohr, Flow Patterns of Two-phase Flow - A Survey of the Literature, Engineering Research Laboratory, Columbia University, TID-11514 (1960).
45. G. B. Wallis and P. Griffith, Liquid and Gas Distributions in a Two-phase Boiling Analogy, Technical Report No. 13, Division of Industrial Research, M.I.T., NP-7204 (1958).
46. M. Wicks and A. E. Dukler, Entrainment and Pressure Drop in Co-current Gas-Liquid Flow; I. Air-Water in Horizontal Flow, A.I.Ch.E.J., 6, 463-468 (1960).
47. N. Zuber, On the Variable-density Single-fluid Model for Two-phase Flow, J. Heat Transfer, Trans. Am. Soc. Mech. Engrs., Series C, 82, 255 (1960).

ACKNOWLEDGEMENTS

The major part of this study was performed at Argonne National Laboratory under the auspices of the United States Atomic Energy Commission through a cooperative arrangement with Northwestern University. Other parts of the work were performed at the University of New Hampshire Computation Center and Chemical Engineering Laboratories.

I would like to express my sincere thanks to Professor S. G. Bankoff of Northwestern University, who introduced me to the problems of two-phase flow and suggested the present investigation; and, in particular, for his many suggestions and criticisms during the course of the study.

I am also grateful to Dr. Paul Lottes of Argonne for his cooperation and counsel; to Dr. Helge Christensen, now at the Institutt for Atomenergi, Kjeller, Norway, for helpful discussions; and to Albert Stogsdill, who helped construct and operate the apparatus, and reduce the data.

Finally, my thanks to Charles Brown, a student at the University of New Hampshire, for taking photographs of the gas bubbles.

ARGONNE NATIONAL LAB WEST



3 4444 00007504 4

M